The Thesis Committee for Brittany Claire Smith
Certifies that this is the approved version of the following thesis:

The effects of vegetation on island geomorphology in the Wax Lake Delta, Louisiana

APPROVED BY
SUPERVISING COMMITTEE:

Supervisor: _____
Kevan Moffett

Co-Supervisor: _____
David Mohrig

_____
Wonsuck Kim

The effects of vegetation on island geomorphology in the Wax Lake Delta, Louisiana

by

Brittany Claire Smith, B.S.

Thesis

Presented to the Faculty of the Graduate School of

The University of Texas at Austin

in Partial Fulfillment

of the Requirements

for the Degree of

Master of Science in Geological Sciences

The University of Texas at Austin

May 2014

Acknowledgements

I would like to thank my advisors, Kevan Moffett and David Mohrig, for their support, patience, thoughtful advice, and positive attitude throughout my time at UT. I feel very fortunate to have had their encouragement and guidance.

Mike O'Connor, Brandon Minton, Christine Bonthius, and Nick Evans were invaluable help in the field, working tirelessly and cheerfully in the face of some very challenging situations. Todd Caldwell, Stacy Slater, and Abigail Black were instrumental in helping me complete my lab analyses in a timely manner. Phil Bennett graciously allowed me to use his lab and equipment even after I broke his muffle furnace. This work benefitted greatly from discussions with Paola Passalacqua, Nathanael Geleynse, and Wayne Wagner, and comments from Wonsuck Kim.

Thank you to my wonderful friends in the Jackson School for your support, laughter, and commiseration. I look forward to being your colleague in the years to come. Thank you to my parents, Rob and Terry Smith, for always encouraging my love of science and never questioning why I would want a career spent playing in the dirt. Finally, thank you to Judy Jarvis for unconditional love and support, and for sharing this adventure with me.

Abstract

The effects of vegetation on island geomorphology in the Wax Lake Delta, Louisiana

Brittany Claire Smith, M.S. Geo. Sci.

The University of Texas at Austin, 2014

Supervisors: Kevan Moffett and David Mohrig

Understanding how deltas build and maintain themselves is critical to predicting how they will respond to perturbations such as sea level rise. This is especially an issue of interest in coastal Louisiana, where land loss is exacerbated due to subsidence and decreased sediment supply. Feedbacks between ecology and geomorphology have been well documented in tidal environments, but the role of vegetation in delta morphodynamics is not well understood. This study investigates spatial and temporal correlations between vegetation succession and sediment accumulation at the Wax Lake Delta in Louisiana. I established a 2500 m long transect along the western levee of Pintail Island, capturing the full range of island elevations and the transition from bare sediment to herbaceous plants and trees. Shallow (50-100 cm deep) sediment cores taken along this transect were analyzed for particle size, organic matter content, and bulk density, and dated using ^{210}Pb. The resulting sedimentation rates and composition trends over time

were compared to remote sensing-based analyses of temporal changes in island topography and flooding frequency derived from historical Landsat images.

We found that the topography of Pintail Island has developed from a non-systematic arrangement of elevations to a discrete set of levees and intra-island platforms with distinct vegetation types, designated as high marsh, low marsh, and mudflat habitat. This elevation zonation is consistent with alternative stable state theory as so far applied to tidal salt marsh systems. At all but the youngest sampling site, sediment cores showed a significant decrease in organic matter content and a significant increase in grain size with depth. The total organic matter contribution to vertical growth was not sufficient to account for all the elevation change required to achieve the differentiation from low marsh to high marsh deduced from the time-lapse Landsat imagery analysis. Mineral sediment accumulation rates suggested that elevation growth was accelerating or holding steady over time, in contrast to theory suggesting rates should slow as elevation increases. These results provide an empirical foundation for future mechanistic models linking mineral sedimentation, organic sedimentation, vegetation succession, elevation change, and flood frequency in the delta.

Table of Contents

List of Tables

List of Figures

1. INTRODUCTION

Understanding how deltas build and maintain themselves is important for predicting how they will respond to perturbations such as sea level rise. Many coastal areas have been retreating or drowning as a result of subsidence and decreased sediment availability due to upstream dams and levees (Kesel, 2003). Ten percent of the world's population lives less than 10 m above sea level and is increasingly vulnerable to flooding and erosion due to sea level rise (McGranahan et al., 2007). Coastal wetland vegetation reduces erosion by attenuating waves and storm surges (Gedan et al., 2011), and proposed efforts to restore deltaic wetlands revolve around diverting currently channelized water and sediment into low lying areas and allowing natural processes to control the development of new wetlands. At this point, knowledge of sedimentary dynamics can evaluate the overall feasibility of these projects, but there is insufficient knowledge to predict in detail how the distribution of elevation, channels, and habitat will evolve (Paola et al., 2011). Though many studies have addressed feedbacks between water flow and sediment transport and deposition in deltas (e.g. Orton and Reading, 1993; Wright and Coleman, 1974; Hoyal and Sheets, 2009; Edmonds and Slingerland, 2007), the role of vegetation in delta geomorphology is not as well understood.

Subaqueous sediment deposition dominates the initial organization of delta islands and channels. Flow expansion and deceleration as channelized flow transitions into a larger body of water induces sediment deposition, forming a mouth bar. Flow splitting around the mouth bar causes channel bifurcation and levee development behind

the bar. The final location of the mouth bar, which sets the initial location for island formation, is strongly controlled by water velocity and depth, and is weakly controlled by grain size (Edmonds and Slingerland, 2007; Van Heerden and Roberts, 1988). Field studies suggest that this jet deposit model initiates mounded island forms with their thickest deposits at the upstream end and along the central island axis (Wellner et al., 2005). However, once these deposits accrete to a level near or above mean water level, emergent plants are able to colonize the islands and vegetation becomes a potential factor in sedimentation dynamics.

Elevation is a geomorphologically and ecologically important variable in tidal and floodplain environments, as it controls depth and frequency of inundation, which in turn affect bed shear stress and the amount and type of sediment delivered to a given location (Cahoon and Reed, 1995; Stoddart et al., 1989; Edmonds and Slingerland, 2009). Deltas exhibit strong morphodynamic coupling between sediment surface elevation, water flow, and sediment deposition or erosion (Hoyal and Sheets, 2009; Kim et al., 2009). It has also been shown that vegetation type and productivity are controlled by elevation in tidal environments via hydrologic regime, resulting in banded vegetation that mirrors local topography (Johnson et al., 1985; Shaffer et al., 1992; White, 1993). However, it is not known if a feedback loop exists between vegetation and elevation in a prograding delta environment, what mechanisms would dominate this interaction, or how this feedback would impact overall delta development.

Numerous examples of field and modeling studies in salt marshes have shown that vegetation influences vertical accretion and erosion (e.g. Kirwan and Murray, 2007;

D'Alpaos, 2011; Mudd et al., 2009; Morris, 2006; Fagherazzi et al., 2012). However, few studies address this issue in freshwater tidal systems. While freshwater tidal systems have similarities to salt marshes, the most notable differences are a lower salinity, higher sediment availability, and greater diversity of plant types, corresponding to the potential for greater spatial variation in geomorphic processes in the freshwater systems (Pasternack and Brush, 2001). Organic matter accumulation is also significantly higher in freshwater marshes due to lower rates of decomposition (Craft, 2007; Lorenzo-Trueba et al., 2012). Nevertheless, given a relative lack of tidal freshwater and delta wetland research, salt marshes are the best analog available.

On a plot scale, the process relationships between vegetation and vertical accretion in tidally influenced systems have been widely studied. Most directly, vegetation contributes organic matter to the subsurface via roots and leaf litter, adding to the overall volume of the soil and increasing the marsh surface elevation. Organic matter contributes up to 4 times more volume than mineral sediment on a per mass basis, due to its lower particle density and higher porosity (Neubauer, 2008). Total accretion rates in coastal marshes have been correlated with organic matter accumulation rates; organic matter has been shown to be the primary driver in many salt marshes while accretion in freshwater marshes is typically a function of both mineral and organic sedimentation (Neubauer, 2008; Nyman et al., 2006; Lorenzo-Trueba et al., 2012). One proposed mechanism explaining this correlation is increased root growth in response to increased inundation (Kirwan and Guntenspergen, 2012; Nyman et al., 2006). One model explicitly accounting for soil carbon dynamics and belowground biomass demonstrated that organic

matter can be a significant factor in maintaining the elevation of salt marshes undergoing sea level rise (Mudd et al., 2009).

Vegetation has also been linked to an increase in net mineral sediment deposition by increasing bed roughness, slowing water velocity and decreasing turbulence. This results in increased deposition through particle settling and a decrease in resuspension (Mudd et al., 2009; Leonard and Luther, 1995; Christiansen et al., 2000). Direct trapping by plant stems may also have a significant effect (Palmer et al., 2004), though others studies find trapping to be negligible compared to settling (Mudd et al., 2009). Regardless of the mechanism, fertilized plot experiments have shown that greater plant productivity in salt marshes creates higher biomass density, which is more efficient at trapping mineral sediment and increasing local elevation (Morris, 2006). Several studies in freshwater marshes have also shown sedimentation rates correlating to vegetation cover, though elevation and proximity to tidal channel are also factors (Palinkas et al., 2013; Pasternack and Brush, 2001) and results have been highly variable (Darke and Megonigal, 2003). Other studies along an elevation gradient show a negative correlation between elevation and mineral accumulation rates in the summer but not winter, suggesting a relationship with vegetation cover (Pasternack and Brush, 2001; Cahoon et al., 2011). However, spatial heterogeneity in vegetation can actually enhance erosion. For example, patchy vegetation may decrease water velocity within the area of plant growth, but focus flow between these vegetated areas, increasing water velocity and erosion in between patches (Vandenbruwaene et al., 2011; Temmerman et al., 2007). Also, sparse vegetation patches may cause an increase in turbulence, resulting in enhanced erosion of

fine grained sediment and creating a sandier surface that is less cohesive (van Katwijk et al., 2010). In general, discontinuous obstructions such as vegetation cause complicated disruptions in the flow field that can extend into vegetation patches, with unpredictable effects (Nepf, 2012).

Plants are expected to affect vertical marsh development by increasing sediment stability through several mechanisms. Root growth typically adds tensile strength and increases soil resistance to shear stress, decreasing surface erodibility (Simon and Collison, 2002) and increasing bank strength (Micheli and Kirchner, 2002; Pollen-Bankhead and Simon, 2010). Cahoon et al. (2011) describe an “explosive” growth of belowground biomass in emergent marsh vegetation, with an order of magnitude increase from submerged sites to low marsh sites in their first several years of colonization, and a correlation between belowground biomass and elevation in the Mississippi River Delta. Additionally, decreased water velocity and turbulence under the vegetation canopy reduces resuspension and erosion (Christiansen et al., 2000) and encourages deposition of finer particles that can potentially increase the cohesion of the sediment surface (Yang, 1998).

The effects of vegetation on delta development over larger spatial or temporal scales are less well understood. Pasternack and Brush (2002) hypothesize that over multidecadal time scales, the cumulative effect of decreased sediment dispersal due to vegetation will result in a shorter, steeper delta. In contrast, experimental and numerical models suggest that increased cohesiveness, potentially supplied by vegetation, results in more stable distributary channels that prograde farther and reach lower gradients than

would otherwise be predicted (Hoyal and Sheets, 2009); more cohesive deltas are expected to be more elongated, with a rougher shoreline (Edmonds and Slingerland, 2009). Similarly, Rowland et al. (2010) describe delta distributary network development as a competition between levee and mouth bar formation, so that more cohesive and stable levees would tend to increase the channel length between bifurcations. On millennial time scales, Lorenzo-Trueba et al. (2012) use a geometric model including organic sedimentation to show that a higher rate of organic accumulation delays shoreline retreat under conditions of base level rise. Models of coupled interactions in salt marshes between abiotic and biotic factors including organic sediment deposition, mineral sediment deposition, and wind induced wave erosion find that the feedbacks between these processes result in alternative stable states where distinct surface elevations are most stable (Marani et al., 2010; D'Alpaos, 2011; D'Alpaos et al., 2012). Because of this tendency for a landscape to approach stable elevations, it has been proposed that multiple peaks in the frequency distribution of elevation corresponding to vegetation zonation in a tidal environment is a signature of feedbacks between ecological and geomorphological processes (Marani et al., 2013).

This study first characterized sediment properties with depth along an elevation gradient on an island in the prograding Wax Lake Delta in Louisiana, with the aim of investigating the influence of vegetation on organic matter accumulation, grain size of deposits, and overall accretion rate. Second, remote sensing imagery was used to determine the topographic change of the delta on a larger scale over time. Finally, local sediment dynamics inferred from evidence preserved in the sediment record were related

to the observed pattern of island evolution. We propose that there are spatial and temporal relationships between vegetation succession and island evolution which reflect a mechanistic link.

2. METHODS

2.1. SITE DESCRIPTION

In 1942, the Wax Lake Outlet Channel was constructed by the US Army Corps of Engineers (USACE), diverting water from the Atchafalaya River upstream from Morgan City, LA for the purposes of flood control. The Wax Lake Delta (WLD) is located where the Wax Lake Outlet flows into the Atchafalaya Bay (Fig. 1a). The USACE Old River Control Structure, located at the convergence of the Red and Mississippi Rivers (Fig. 1a), diverts 30% of the flow from the Mississippi River to the Atchafalaya River; the Wax Lake Outlet contains up to 46% of the flow from the Atchafalaya (Allison et al., 2012). The delta has been developing subaqueously since 1952, and became subaerial after a large flood in 1973 (Rouse et al., 1978) . Consisting primarily of sand rich deposits on top of the original consolidated mud bay surface, the delta has now built out into the bay approximately 10 km (Rouse et al., 1978; Roberts, 1997). Terrain and morphodynamic models suggest progradation at a rate of 3-5 km^2/yr (Parker and Sequeiros, 2006). The delta is a low gradient system, with the entire subaerial portion within 1 m of mean water level (NCALM, 2009) and is tidally influenced, with an average tidal amplitude of 60 cm (NOAA, 2013), though river discharge and wind also factor into water level (Geleynse et al., in review; Hiatt et al., in review). Though the delta extends into Atchafalaya Bay, it is surrounded by freshwater due to the large volume of water discharging from the Wax Lake Outlet. Due to its small size, relatively good historical record, and lack of substantial engineering (Roberts, 1997), the WLD is an ideal place to study delta dynamics.

Pintail Island was selected for study (Fig. 1c). The island shape is characteristic of the delta, with an arrowhead-shaped pair of levees and a lower, wetter area in the middle of the island open to the channel at its downstream end. Based on historical imagery, Pintail is one of the older islands in the delta so it was expected to have a relatively complete sedimentary record encompassing the lifetime of the delta, while still actively growing and changing. To capture variations in elevation, we established 5 sites along a 3 km transect of the western levee of Pintail Island, from the highest elevation at Site 1 to the lowest elevation at Site 5 (Fig. 1c, d). Each sampling site was a similar distance from the channel. Sites 1, 2, 3, and 5 all had clusters of *Salix nigra* trees present in addition to herbaceous cover between the tree patches. These sites were sampled within both the tree clusters and the dominant herbaceous vegetation representative of the area. Sites are denoted by their number and T (trees) or H (herbaceous). At Sites 1-3, the dominant herbaceous vegetation was *Colocasia esculenta.* Site 4 was selected to capture a drop in elevation below the small channel just south of Site 3, had no trees, and the main vegetation type was *Typha* spp. At Site 5, the dominant herbaceous species was *Schoenoplectus americanus*.

Figure 1: Site description. A) The Wax Lake Delta is located at the terminus of the Wax Lake Outlet (blue), which diverts water from the Atchafalaya River (purple). The Atchafalaya is a distributary channel for the Mississippi (green) and Red (red) Rivers. B) Landsat image of the WLD. The yellow dot indicates the location of the USGS gage at Camp Island, and the dashed line shows the location of the water surface transect in Figure 4c. The white box indicates the location of (C). C) False color NIR-R-G aerial photo of Pintail Island from Nov. 6, 2009 with location of 5 core sampling sites. The dashed line indicates the location of the elevation transect in (D). D) Elevation transect from 2009 Lidar data (NCALM, 2009) down the western levee of Pintail Island, with the elevation of each sampling site noted.

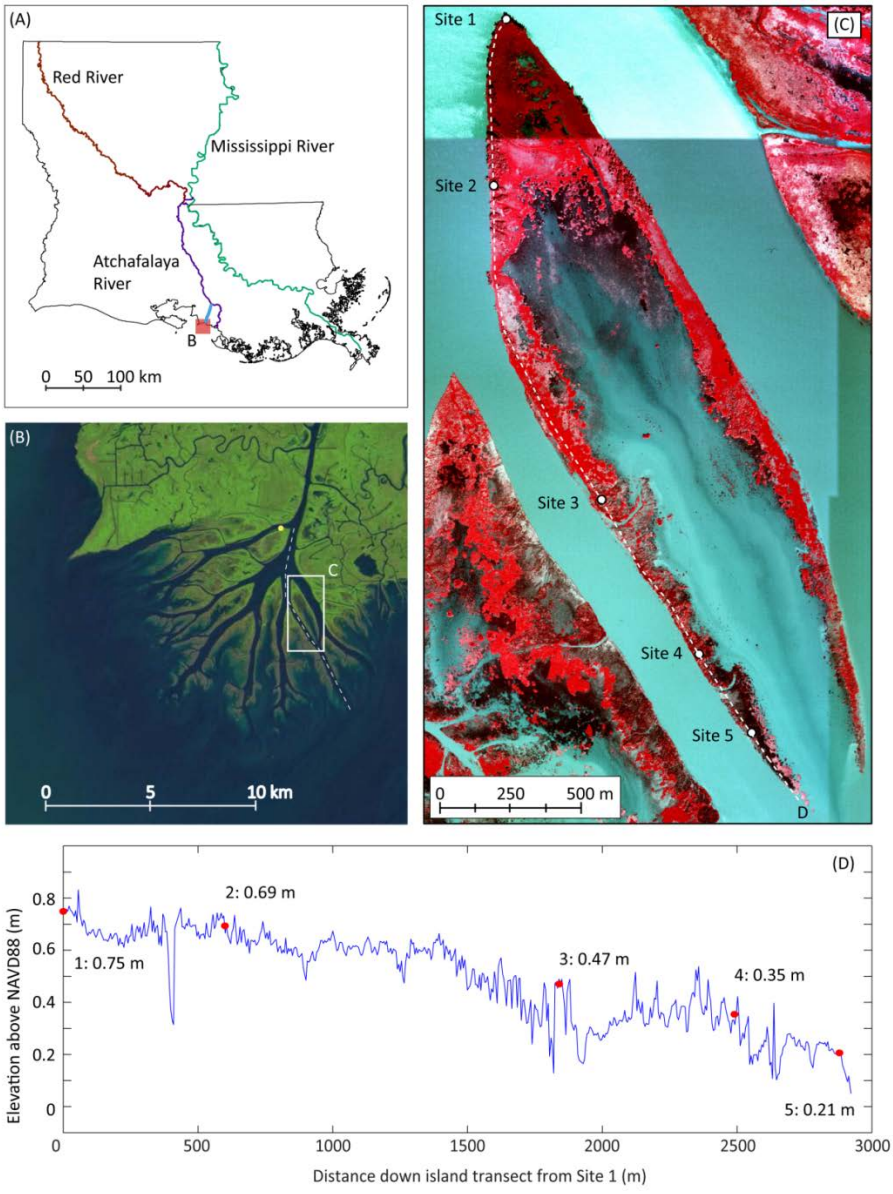

The two vegetation types were chosen to remove elevation as a variable, and to capture vegetation at different levels of productivity, which is expected to be a factor driving marsh development. In the vegetation zone classification scheme described by Viparelli et al. (2011), *S. nigra* is considered "high woody," *C. esculenta* is "high emergent," and *S. americanus* is "intermediate emergent" (Fig. 2). Specific elevation data on *Typha* spp. are not available, but other work in the Atchafalaya Basin suggests it fits best in the "intermediate emergent" community (Johnson et al., 1985; Shaffer et al., 1992). The low elevation island interior is dominated by *N. lutea*, a "low emergent" species.

Figure 2: Vegetatation percent cover as a function of community type and elevation above mean sea level at the Wax Lake Delta, after Viparelli et al. (2011). The species in each community are as follows: Trees (Salix nigra), High Emergent (Colocasia esculenta, Polygonum punctatum,Vigna luteola), Intermediate Emergent (Schoenoplectus americanus, Alternanthera philoxeroides, Leersia oryzoides), Low Emergent (Sagittaria platyphylla, Nelumbo lutea), Submerged (Potamogeton nodosus).

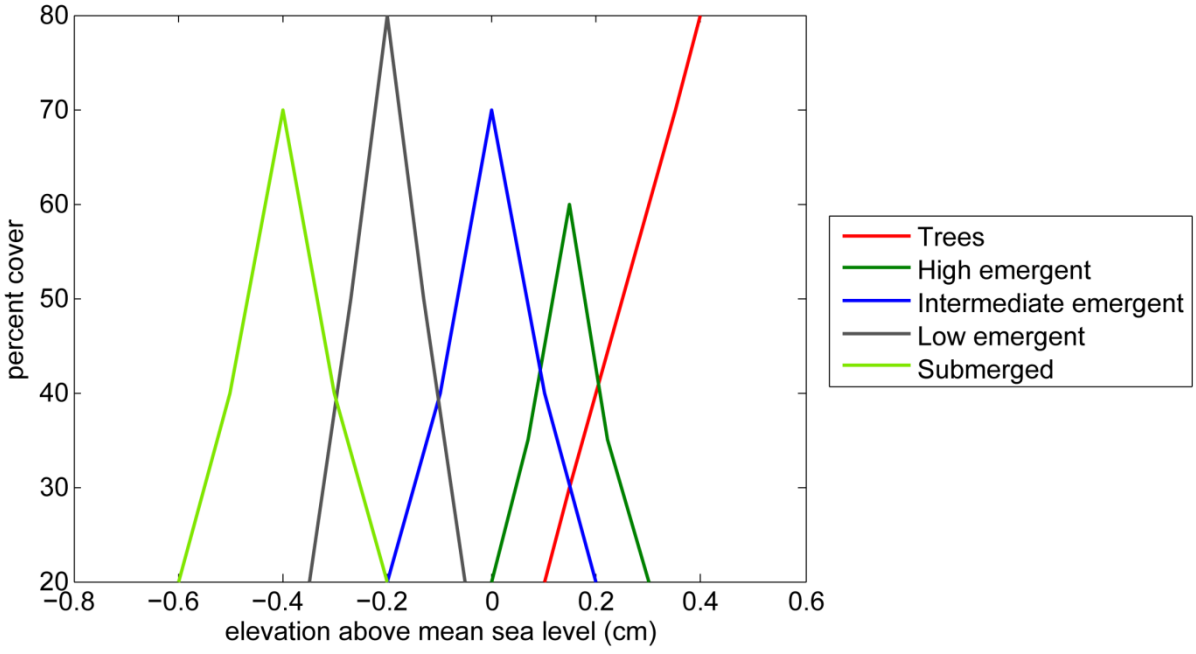

2.2. FIELD METHODS

In September and November 2013, at each site and within each vegetation type, 3 replicate sediment cores were taken ranging in length from 40 to 85 cm. Preliminary field investigations suggested a transition from mud to sand near mean water level, which varied with elevation. The intention was to core to below this depth, so shorter cores were taken at the lower elevation sites. Push- cores were taken using a sharpened PVC pipe 5 cm in diameter with an airtight piston to provide suction and prevent core material from falling out the bottom as it was extracted from the ground (Hargis and Twilley, 1994). The cores were capped in the field, and transported upright to the laboratory. Compression with depth was determined in situ during coring by measuring the depth to the soil surface both inside and outside the coring device every 5 cm while inserting the PVC pipe into the ground. To provide an additional indicator of vegetation history on the island, tree cores were taken from 13 of the largest *S. nigra* trees near Sites 1-3 using an increment borer, and annual rings were counted for approximate date of establishment (Stokes and Smiley, 1968). The trees at Site 5 were too small to bore, but two trees were cut and sectioned to obtain ages.

2.3. LABORATORY METHODS AND ANALYSIS OF SEDIMENT CORES

The sediment cores were cut open lengthwise in the laboratory using a rotary hand tool and sectioned every 2 cm, weighed, dried for 24 hours in a 105°C oven and reweighed. Each section was sub-sampled for organic matter content, particle size, and Pb-210 analyses. Because significant compression occurred in the cores, a correction

was applied to convert depth in the core to depth below the surface for each core section. The difference between the depths to the sediment surface measured inside and outside the PVC pipe every 5 cm while coring were linearly interpolated between each measurement point and used to correct the in situ depth to the top and bottom of each core section. The results of this study are stated in terms of these corrected in situ depths.

2.3.1. Organic Matter

Organic matter content by mass ($\%OM_{mass}$) for each slice was measured using the loss on ignition method, where oven dry samples were weighed, heated to 450 $^{\circ}$C for 16 hours, and reweighed (Craft, 2007; NRCS, 2004). The volume of the organic V_{om} (Eqn. 1) and mineral V_{min} (Eqn. 2) sediment fractions were computed for each core section using assumed particle densities of 1.25 g/cm^3 (ρ_{om}) and 2.65 g/cm^3 (ρ_{min}) for the organic and mineral components (Rühlmann et al., 2006), and the total dry mass of each section, M_{tot}. The % OM by volume ($\%OM_{vol}$) was calculated for each core using Equation 3. The bulk density of each slice ρ_b was also found (Eqn. 4) using the corrected height for each section, Z_s.

$$V_{om} = M_{tot} * \frac{\%OM_{mass}}{100} * \frac{1}{\rho_{om}} \quad (1)$$

$$V_{min} = M_{tot} * (1 - \frac{\%OM_{mass}}{100}) * \frac{1}{\rho_{min}} \quad (2)$$

$$\%OM_{vol} = \frac{V_{om}}{V_{om}+V_{min}} * (100) \quad (3)$$

$$\rho_b = \frac{M_{tot}}{Z_s * 2.5^2 * \pi} \quad (4)$$

The total vertical contribution of organic matter (Z_{om}) to each core was calculated using Equation 5, where *n* is the total number of sections in the core.

$$Z_{om} = \sum_{i=1}^{n} Z_s(i) * \frac{\%OM_{vol}(i)}{100} \quad (5)$$

Statistical analyses were performed on the organic matter data, which included data from three replicate cores from each site and vegetation type. For each coring location, the median value for % OM by volume was linearly interpolated every 2 cm between adjacent measured slices (which were irregularly spaced due to nonlinear compression). A Mann-Kendall test was applied to each triplicate of cores at each site to test for a trend in the profile. The test is non-parametric and does not assume a linear trend. A Wilcoxon rank sum test was used to compare herbaceous site to tree site organic matter profiles both above and below mean local water level (MLWL) at Sites 1-3. At Site 4 the test was not applied because there was no tree site. In Site 5 the rank sum test was only applied below MLWL because no part of the cores was above MLWL. The total vertical contribution Z_{om} was normalized by core length and a Students t-test compared the distribution of total organic matter values between herbaceous and tree cores at each site.

2.3.2. Grain Size

Prior to grain size analysis, samples with greater than 2% organic matter by mass were pre-treated with 25 ml of 30% hydrogen peroxide and heated at 85 $^{\circ}$C for 2 hours to digest organic matter. Digested and non-digested samples were shaken overnight on a reciprocal shaker with 20 ml of 0.25 M sodium hexametaphosphate dispersing solution (NRCS, 2004), and measured using a Malvern Mastersizer 3000 laser particle size

analyzer (Zobeck, 2004). Like the organic matter data, at each coring location the median value for D_{50} with depth was linearly interpolated every 2 cm between adjacent measured slices. A Mann-Kendall test for trends was applied to each core, and a Wilcoxon rank sum test was used to compare herbaceous site to tree site grain size profiles both above and below MLWL at Sites 1-3 and 5.

2.3.3. ^{210}Pb Analysis

Sections of the sediment cores were dated using Pb-210 dating. Pb-210 has a half life of 22.26 years and is good for dating sediment deposited within the last 100-150 years (Appleby and Oldfield, 1983), so was appropriate for this site which has a maximum age of 60 years. ^{210}Pb is a daughter product of the ^{238}U decay series occurring in minerals. Sediment contains some background ^{210}Pb from this in situ decay, which is in equilibrium with its precursors. ^{222}Rn is produced as an intermediate isotope in the decay series, some of which diffuses into the atmosphere where it decays to ^{210}Pb. Of interest for dating is the ^{210}Pb in the atmosphere, which falls onto the land or water surface, where it adsorbs to sediment particle at the surface as excess unsupported ^{210}Pb (Appleby and Oldfield, 1983). Although this atmospheric ^{210}Pb fallout rate is somewhat variable, it is much less so than the variations in sediment deposition rates, making the magnitude of excess ^{210}Pb a useful proxy for sediment deposition rates. If mineral sediment accretion is slow, excess ^{210}Pb will be larger as it has longer to accumulate at the surface; a layer that is accreted quickly will have lower excess ^{210}Pb (Appleby, 2008).

The least compressed core from each sampling location was selected for ^{210}Pb analysis, and alternating slices were analyzed, excluding the first and last slice. Following the methods of Aalto and Nittrouer (2012), 1-1.5 g of sample was spiked with 1.0 ml of ^{209}Po (93.87 mBq ml^{-1}) and acid leached by 8M HNO_3, evaporated, acid leached again with 6M HCl, and re-evaporated. Samples were rinsed, centrifuged, and the supernatant decanted. Ascorbic acid and 0.5 M HCl were added, and polonium was plated on a silver plating planchet suspended in solution for 24 hours. The plated sample was counted in an alpha spectrometer for 24 hours to measure the activity of ^{210}Po, which is assumed to be in secular equilibrium with ^{210}Pb.

Sediment accumulation rates were found using the constant rate of supply (CRS) model as described by Appleby and Oldfield (1978, 1983) and successfully applied in multiple environments (Appleby, 2008; Neves et al., 2014; He and Walling, 1996). This method assumes excess ^{210}Pb is being deposited from the atmosphere onto the sediment surface at a constant rate, but allows for temporal variation in sediment accumulation rate. The unsupported excess ^{210}Pb concentration at depth *x* is represented as *C(x)* in units of decays per minute (dpm)/g, where sediment with concentration *C(x)* of age *t* is a function of the initial concentration C_0 (Eqn. 6). Because ^{210}Pb is primarily adsorbed by clay particles, excess ^{210}Pb was normalized to $C(x)_c$ by the 2 micron clay content to account for the variable clay fraction (f_c) throughout the core (Eqn. 7).

$$C(x) = \mathrm{C_0 e^{-kt}},\ units = dpm/g \tag{6}$$

$$C(x)_c = \frac{C(x)}{f_c},\ units = dpm/g_{clay} \tag{7}$$

Where *k* is the decay constant for ^{210}Pb:

$$k = \log\frac{2}{22.26} \approx 0.3114,\ units = yr^{-1} \quad (8)$$

A(x) is the total unsupported excess ^{210}Pb beneath depth *x*, where $\rho(x) = M_{mineral}/V_s$ for each core section:

$$A(x) = \int_x^{\infty} \rho(x) C(x)_c dx,\ units = \frac{dpm * g_{min}}{cm^2 * g_{clay}} \quad (9)$$

A(0) is the total unsupported excess ^{210}Pb in the sediment column:

$$A(x) = A(0)e^{-kt} \quad (10)$$

t is the age of sediment at depth *x*, where *A(0)* and *A(x)* are solved by numerical integration of the ^{210}Pb activity profile with depth:

$$t = \frac{1}{k}\ln\frac{A(0)}{A(x)},\ units = yr \quad (11)$$

The sedimentation rate *r(x)* associated with sediment at depth *x* was calculated with Equation 12:

$$r(x) = \frac{kA(x)}{C(x)_c \rho(x)},\ units = \frac{cm}{yr} \quad (12)$$

A Mann-Kendall test for trends was applied to each core, and a Wilcoxon rank sum test was used to compare herbaceous site to tree site mineral accumulation rate profiles both above and below MLWL at Sites 1-3 and 5.

2.4. REMOTE SENSING ANALYSIS

There is little historical topographic information available for the WLD, and this study had access only to one Lidar dataset at 1 m horizontal resolution from 2009 (NCALM, 2009). However, there is an extensive set of Landsat satellite imagery at 30 m

horizontal resolution available from 1999-2010 (NASA, 2010). This study takes advantage of the fact that water level fluctuations have a large effect on how much of the delta is exposed at any given time (Fig. 3). Each Landsat image is taken at a different, unknown, random water level, so each shows a different area of the delta. Previously, remote sensing techniques have been primarily used in deltaic coastal environments to monitor spatial extent and land cover, without accounting for the effects of changing water level (Rosen and Xu, 2013). Recent work at the WLD has characterized the variability associated with using satellite imagery to measure land extent change over time, but does not address vertical change (Allen et al., 2011). Other researchers have used a series of satellite images to construct an elevation model based on tidal inundation, but this "waterline" method relies on known water levels at the time the images were taken (Ryu et al., 2008; Mason et al., 2010). In this case, the specific water levels for each image are not available, and there is no existing model for predicting water level at this site in sufficient detail, as it is a function of tidal cycles, river discharge levels, and local wind direction (Geleynse et al., in review). Therefore, this study developed a method to use information contained in Landsat imagery to characterize the topography of the delta from 1999-2010 as calibrated using the Lidar dataset from 2009 (NCALM, 2009).

2.4.1. Landsat waterline method

Landsat images of the WLD were acquired from the USGS Earth explorer website for the years 1999-2010, from Path 23, Rows 39 and 40 (NASA, 2010). The 79 cloud free

available Landsat images were divided into four groups, each spanning 3 years: 1999-2001 (n=17), 2002-2004 (n=19), 2005-2007 (n=19), and 2008-2010 (n=24) (Table 1). The Landsat images in each group were converted into binary images where land=1 and water=0, using the Otsu thresholding method (Otsu, 1979) on either the red band (RGB images) or Band 5 (multiband images), after Geleynse et al. (2012). Each group of binary images were then added together, creating a composite image with pixels ranging in value from 0 to n, where n equals the number of images in that 3-year time period. These pixel values indicate relative frequency of land exposure, such that locations with a land exposure value of 0 were areas that were always water, while pixels of value n indicated areas that were never flooded during the Landsat observation times. Each land exposure value was then converted to a probability of exposure by dividing by the maximum value for each image (n). This study refers to these maps as the "raw Landsat exposure probability maps."

Figure 3: Example of the difference in land exposure as a result of small differences in water levels. In a), the daily average water level at the Camp Island gage station (Fig. 1b) was 0.35 m, and in b) the gage level was 0.67 m (0.32 m difference).

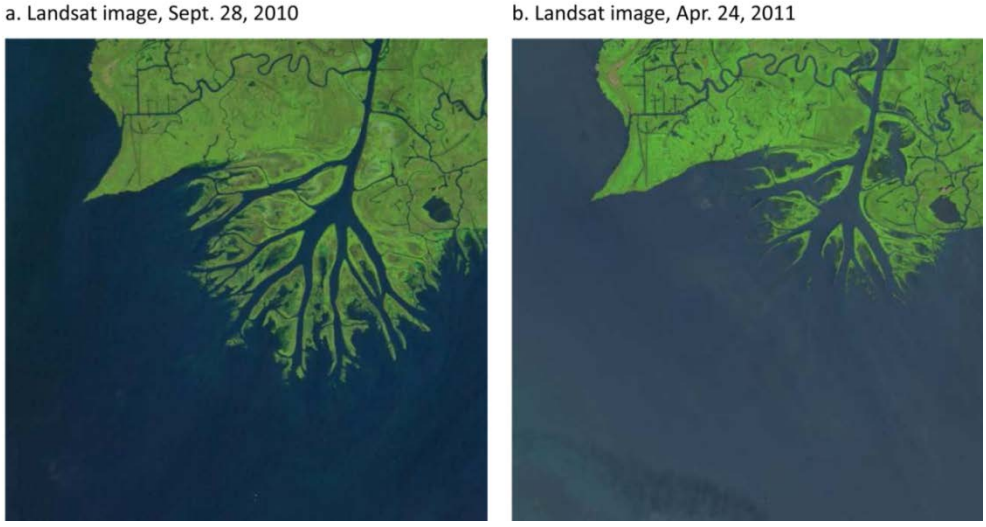

Table 1: Dates of Landsat imagery compiled for each composite image

1999-2001 (n=17)	2002-2004 (n=19)	2005-2007 (n=19)	2008-2010 (n=24)
July 4, 1999	January 25, 2002	January 17, 2005	February 27, 2008
August 5, 1999	February 10, 2002	September 30, 2005	March 30, 2008
August 21, 1999	June 18, 2002	October 16, 2005	April 15, 2008
September 6, 1999	August 5, 2002	November 17, 2005	May 01, 2008
September 22, 1999	August 8, 2002	February 05, 2006	June 02, 2008
October 24, 1999	September 25, 2003	April 10, 2006	September 22, 2008
November 9, 1999	November 28, 2003	June 13, 2006	October 08, 2008
January 12, 2000	December 30, 2003	August 16, 2006	November 09, 2008
February 29, 2000	February 16, 2004	September 01, 2006	November 25, 2008
April 17, 2000	April 4, 2004	November 04, 2006	January 12, 2009
May 19, 2000	May 6, 2004	November 20, 2006	March 01, 2009
June 4, 2000	May 22, 2004	December 06, 2006	May 20, 2009
June 20, 2000	July 25, 2004	March 28, 2007	August 08, 2009
September 24, 2000	August 10, 2004	April 29, 2007	August 24, 2009
October 26, 2000	September 11, 2004	June 16, 2007	November 12, 2009
November 27, 2000	September 27, 2004	July 02, 2007	February 16, 2010
December 29, 2000	October 13, 2004	August 03, 2007	June 08, 2010
March 19, 2001	October 29, 2004	September 04, 2007	July 10 , 2010
	December 16, 2004	September 20, 2007	August 27, 2010
			September 12, 2010
			September 28, 2010
			October 14, 2010
			October 30, 2010
			December 01, 2010

Daily averaged surface water level data from USGS gage 073815925 (29°32'24" N, 91°26'08" W), located at Camp Island (Fig. 1b) at the apex of the delta, was acquired from the US Geological Survey National Water Information Service website (U.S. Geological Survey, 2014) for the period of record from 10/15/2008-1/12/2014. The mean surface water level at the gage for this period was 0.481 m above NAVD88, reaching a maximum level of 1.12 m and a minimum level of -0.11 m (Fig. 4a). The cumulative

distribution of water levels throughout this period was fitted with a cumulative normal distribution with a mean of 0.481 m and a standard deviation of 0.179 (Fig. 4b). To more accurately extrapolate this gage data to the surroundings of Pintail Island, 2.5 km or more away, a transect of surface water elevations was extracted from the Lidar 2009 dataset along the path of water travel from the head of Camp Island down the channel to the west of Pintail Island (Fig. 1b). A line was fit to the transect to determine the surface water slope, and an average slope of -4.7×10^{-5} was calculated from the linear regression (Fig. 4c). The distance from each pixel in the Lidar 2009 dataset to the gage station was calculated. This distance and the surface water slope were used to calculate the MLWL corresponding to each point in the Lidar 2009 dataset. This MLWL value was subtracted from the land surface elevation value at each point, converting the Lidar datum to land surface elevation above MLWL. The CDF of water level elevation was also converted to a MLWL datum by subtracting the mean, so that the converted distribution had a mean of 0 and standard deviation remained the same. For each value of elevation above MLWL in the Lidar dataset, the probability of non-exceedance by surface water flooding was calculated from the CDF relationship. This is referred to the "Lidar 2009 exposure probability map" since the probability of non-exceedance is equivalent to the probability of exposure under the water level regime captured by the Camp Island gage period of record and the 2009 Lidar topography acquisition.

Figure 4: Surface water data. A) Surface water hydrograph from the USGS gage 073815925 period of record at Camp Island (Fig. 1b), with mean water level of 0.481 m indicated by dashed line. B) Cumulative distribution function of water levels derived from a), with fitted normal cumulative distribution function with parameters mu=0.4811 m and sigma=0.179 m. C) water surface transect (Fig. 1b) down delta derived from 2009 Lidar, and fitted with a linear regression with a slope of -4.7 E-5.

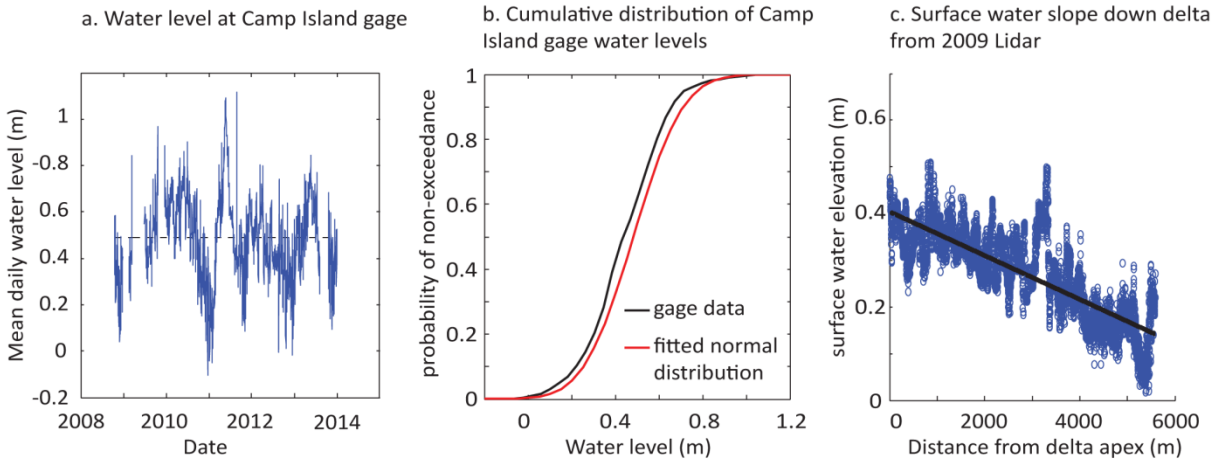

This 1 m resolution Lidar 2009 exposure probability map was overlain by the 30 m resolution raw Landsat exposure probability map from 2008-2010. It was determined that the areas with Landsat exposure probability values of 0.04-0.29 were not captured in the Lidar dataset because these values were primarily in the low-lying center of the island which was not exposed at the time the Lidar data were acquired, so these values were removed for the purpose of this analysis. A linear regression was fit to the relationship between the Lidar and Landsat exposure probability datasets. This linear relationship was then applied to the other three Landsat datasets to correct the initial, raw Landsat-based estimates of exposure probability to new "corrected Landsat exposure probability maps". This correction was necessary because the departure of the Lidar-to-Landsat regression

from a 1:1 line and slope of 1 indicated that the raw Landsat exposure probability estimation method may have included some bias. By applying this regression to the raw Landsat estimates, the bias was removed to the extent possible. These corrected Landsat exposure probability maps and the CDF relating water level and probability of exceedance (Figure 4b) were then used to calculate the water elevation at which each Landsat pixel would flood, i.e. its elevation above MLWL. MLWL was calculated for each pixel according to its distance from the Camp Island gage and the surface water slope (Figure 4c, assumed constant on average), and was then added to the elevation above MLWL value. This series of calculations resulted in create maps of elevation above NAVD88 based on the three older Landsat datasets. After completing this Landsat waterline method, histograms of the Landsat elevation distributions were calculated for each time period (1999-2001, 2002-2004, 2005-2007, and 2008-2010).

3. RESULTS

3.1. CORE DATA

3.1.1. Organic matter content

The older, higher elevation sites (Sites 1-4) showed a significant trend of increasing organic matter content with decreasing depth in sediment cores collected from both vegetation types, while the lower distal site (5H, 5T) did not show a significant trend (Table 2). Sites 1 and 3 had significantly different organic matter profiles between vegetation types above MLWL, with 1H and 3H having overall higher organic matter content (Table 2). Though the median profiles of Site 2 look different, it is not significant ($p<0.5$). Comparing vegetation types within each site, only Sites 3H and 3T had a significantly different total organic matter content as a percentage of the length of the core, with a p value of 0.01 (Fig. 7). Despite the range in elevation from Site 1 to 3 and corresponding theoretical range in *C. esculenta* vegetation productivity, the overall organic matter profiles at Sites 1-3H were very similar (Fig. 6d), as well as the total organic matter contribution to vertical growth (Fig. 7). Within the tree sites, 2T had a much higher organic matter profile than the other 3 tree sites, even Site 1 which has trees of a similar age (Fig. 6a, Table 5). Cores at Site 2T and 2H also had the highest overall total organic matter contributions as a percentage of core length, 9.5% and 10.3% respectively (Fig. 7).

3.1.2. Grain size

Similar to the organic matter profiles, sediment cores from Sites 1-4 all had a significantly decreasing grain size trend with decreasing depth, while the Site 5 grain size profiles did not have a significant trend (Table 3). There was variability around this trend, such as the abrupt increase in D_{50} in Site 1T at 40 cm depth and in Site 2T at 35 cm depth, but the overall pattern of fining upward was clear. Sites 1 and 3 are the only sites with significantly different D_{50} profiles between vegetation types above MLWL, while Sites 2 and 5 had significantly different D_{50} profiles between vegetation types below MLWL. Overall, the grain sizes at Pintail Island were very fine sand or finer, and a large proportion of the core sediments had a D_{50} falling below the 62 micron maximum for silt (Fig. 5).

3.1.3. ^{210}Pb dating

At Sites 1-4, locations among both vegetation types showed a significant trend of increasing mineral sediment accumulation rate with decreasing depth, while Site 5 had no significant trend (Table 4). There was variability around this trend at all sites, in particular at Sites 2H, 3H and 4H which all showed abrupt increases and decreases in accumulation rate. The overall highest sustained rates of 5-7 cm/yr were associated with the upper 30 cm of Site 3H; otherwise rates at Sites 1-4 typically range from 0.1 to 3 cm/yr. Sites 5H and 5T varied from 0.1 to 1 cm/yr.

Figure 5: Summary of sediment core data. Each row is one site location. Blue lines are tree sites, red lines herbaceous. Dashed black line is mean local water level for each site. Column 1 shows organic matter by volume (median of three replicate cores), Column 2 shows D_{50} grain size (median of three replicate cores), and Column 3 shows sediment accumulation rates derived from Pb-210 (single core). Site 4 had no trees in the vicinity.

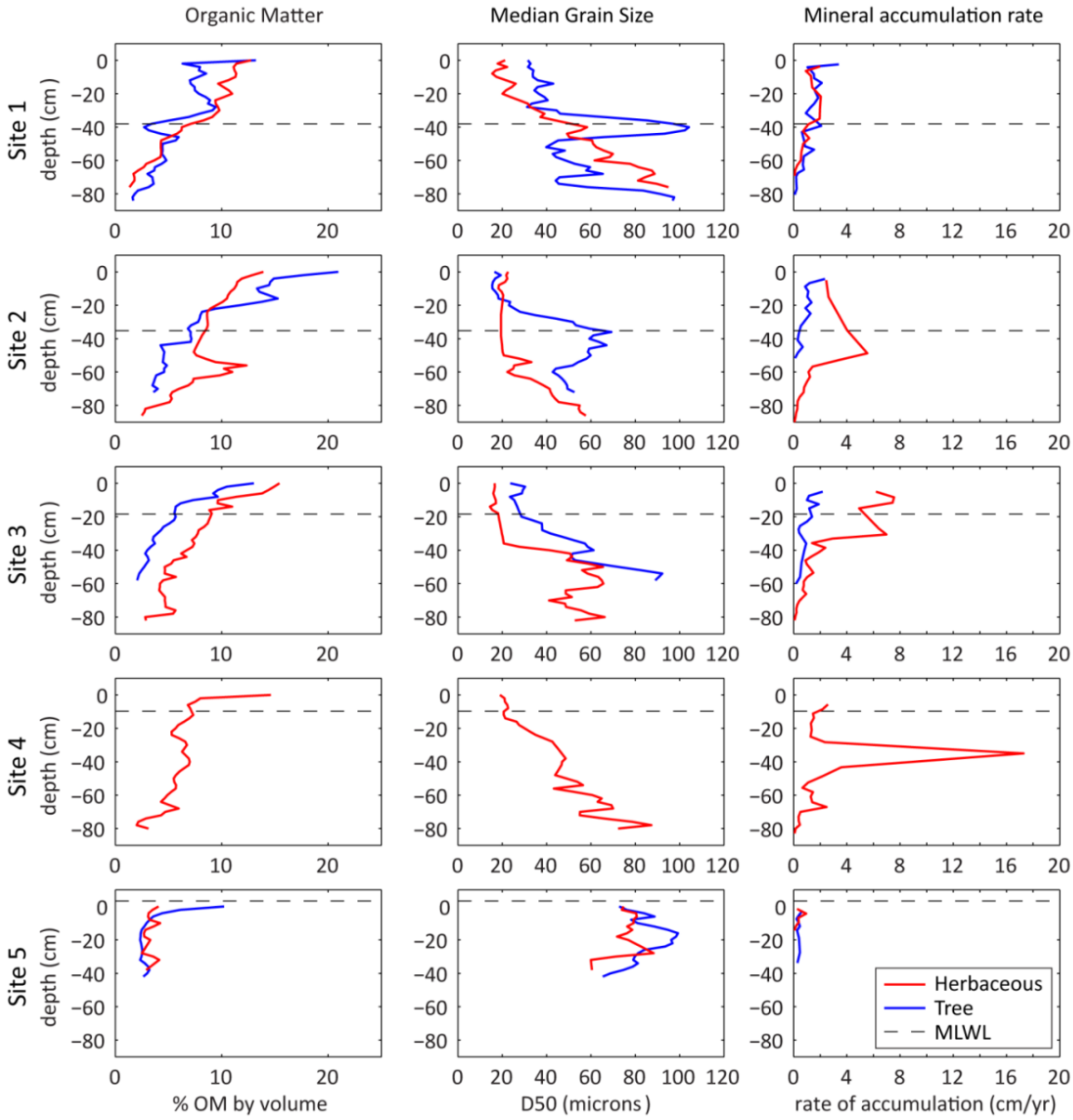

Figure 6: Sediment core data from each site displayed by vegetation type. a) and d) are tree and herbaceous % organic matter by volume (median of three replicate cores). b) and e) are tree and herbaceous D_{50} grain size (median of three replicate cores). c) and f) are tree and herbaceous sediment accumulation rates derived from Pb-210 data (single core). Site 4 had no trees in the vicinity.

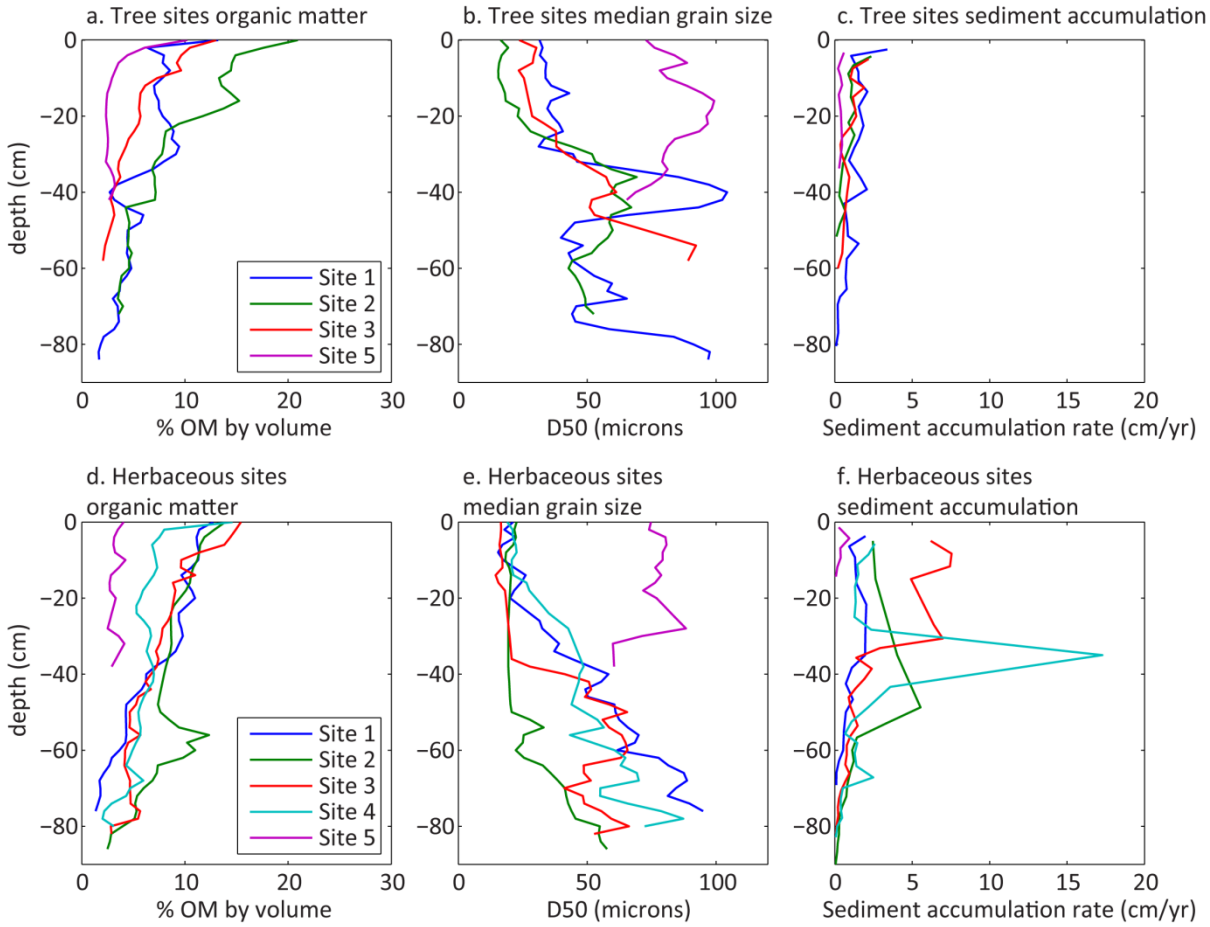

Table 2: Statistical analyses of organic matter profiles. Results of Wilcoxon rank- sum test comparing distributions above and below MLWL, and results of the Mann-Kendall test test for a trend on the median organic matter profile. p values are reported, and p values < 0.05 are marked in white, indicating rejection of the null hypothesis of no difference (Wilcoxon) or no trend (Mann-Kendall).

	Wilcoxon rank-sum test		Mann-Kendall test for trend	
site	H vs. T above MLWL	H vs. T below MLWL	Herbaceous	Trees
1	4.17E-05	0.883	3.77E-11	2.75E-08
2	0.119	0.141	7.01E-12	3.64E-08
3	0.049	0.030	7.51E-12	5.57E-05
4	No trees	No trees	9.75E-08	No trees
5	Not above MLWL	0.089	0.82	0.56

Figure 7: Vertical contribution by organic matter. Total organic matter in each core is reported as % of total core length

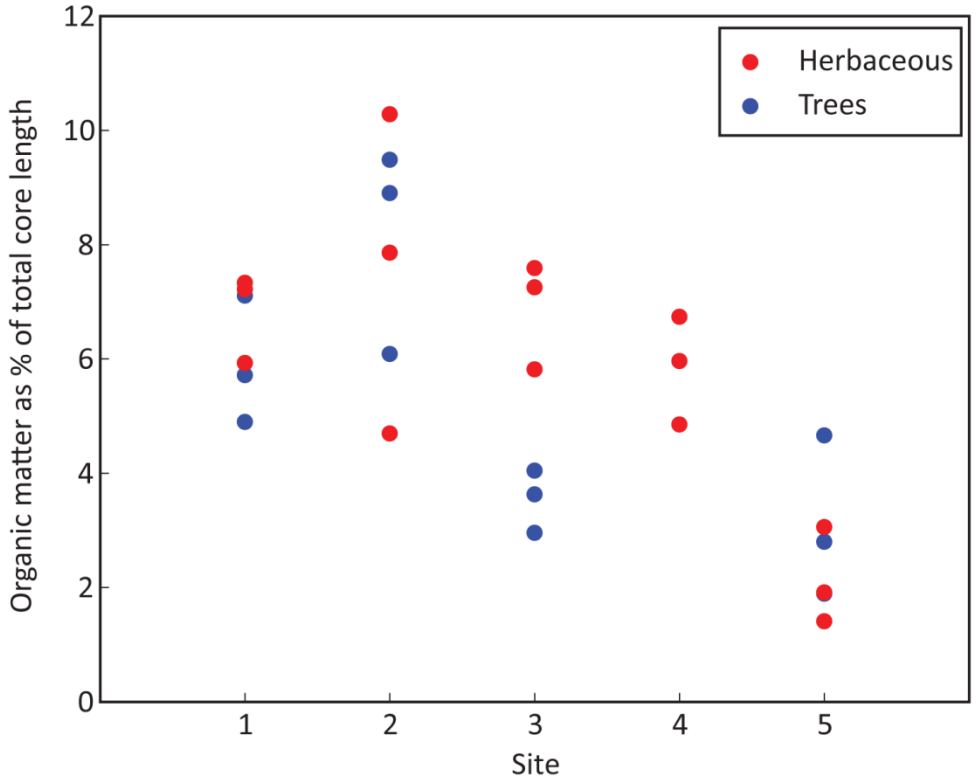

Table 3: Statistical analyses of grain size profiles. Results of Wilcoxon rank- sum test on D_{50} grain size data comparing distributions above and below MLWL, and results of Mann-Kendall test on median D_{50} profile. P values are reported, and p values < 0.05 are marked in white, indicating rejection of the null hypothesis of no difference (Wilcoxon) or no trend (Mann-Kendall).

	Wilcoxon rank-sum test		Mann-Kendall test for trend	
site	H vs. T above MLWL	H vs. T below MLWL	Herbaceous	Trees
1	1.73E-05	0.811	1.79E-10	3.54E-06
2	0.504	0.003	4.25E-07	3.45E-03
3	3.59E-05	0.428	3.89E-09	5.34E-04
4	No trees	No trees	2.37E-11	No trees
5	Not above MLWL	0.001	0.72	0.60

Table 4: Statistical analyses of mineral accumulation rates. Results of Wilcoxon rank-sum test comparing distributions above and below MLWL, and results of the Mann-Kendall test for a trend. P values are reported, and p values < 0.05 are marked in white, indicating rejection of the null hypothesis of no difference (Wilcoxon) or no trend (Mann-Kendall).

	Wilcoxon rank sum test		Mann-Kendall test for trend	
site	H vs. T above MLWL	H vs. T below MLWL	Herbaceous	Trees
1	0.73	0.69	4.63E-04	3.57E-05
2	0.01	0.43	1.05E-07	1.50E-03
3	0.02	0.18	4.00E-10	1.54E-03
4	No trees	No trees	4.02E-04	No trees
5	Not above MLWL	0.39	0.26	0.75

3.2. REMOTE SENSING

3.2.1 Verifying the Landsat exposure probability data as a predictor of elevation

The Lidar 2009 elevation dataset for Pintail Island (Fig. 8a) was converted to The Lidar 2009 exposure probability map (Fig.8b) and compared to the raw Landsat exposure

probability map created from images from 2008-2010 (Fig. 8c). The intra-island platform in the Lidar maps (8a, b) is under water, while it is shown as land in the Landsat exposure probability map (8c) because the Landsat map includes images taken at water levels lower than occurred during Lidar data acquisition. Using linear regression, the Lidar 2009 exposure probability data and from the raw Landsat exposure probability data were related by the monotonic trend:

(Lidar exposure probability)=1.1947*(Landsat exposure probability)-0.2529 (13)

with $r^2 = 0.973$. In calculating the relationship between Lidar and Landsat exposure probability, the difference in resolution between the two datasets (1 m and 30 m respectively) meant that each Landsat pixel contained up to 900 Lidar pixels. Since many topographic features on Pintail Island are smaller than 30 m, this resolution difference introduced a large amount of scatter within each group of Lidar pixels associated with a given value of Landsat exposure probability. The linear regression was fit to all the data (not shown), rather than the median probability of exposure values (shown, Fig. 9).

Figure 8: Elevation and exposure probabilities for Pintail Island. a) Pintail Island elevations from Lidar 2009 dataset. b) Pintail Island probability of exposure calculated from Lidar elevation, linear water surface slope (Fig. 4c), and fitted water level distribution (Fig. 4b). c) Probability of exposure map calculated using 24 Landsat images from 2008-2010.

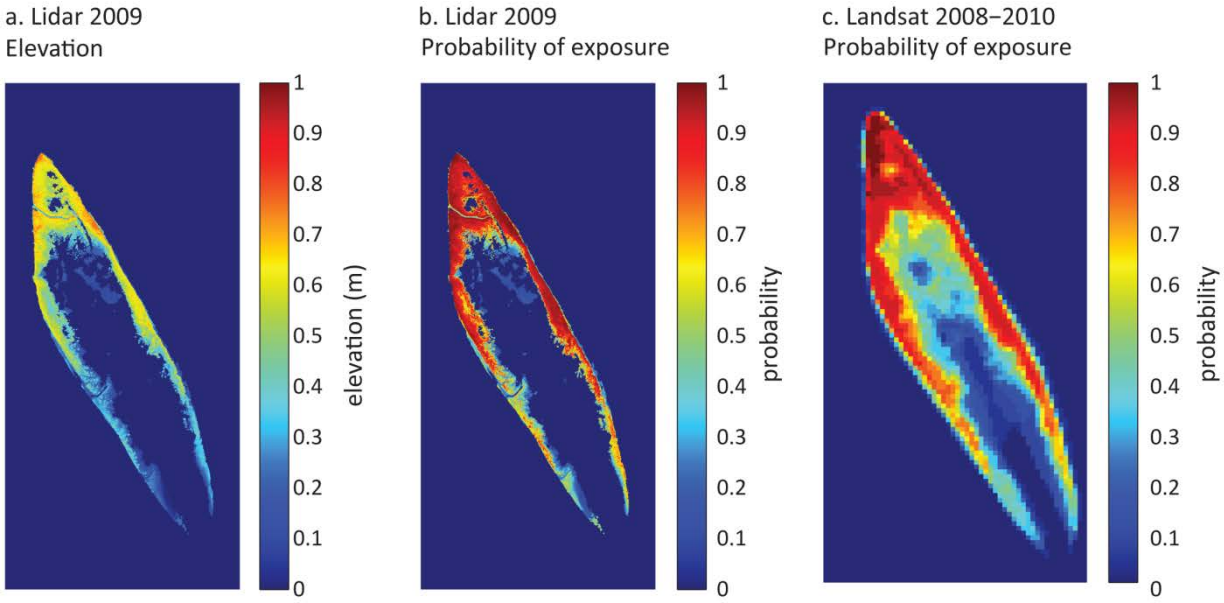

Figure 9: Probability of exposure calculated from Lidar 2009 (y-axis) and spatially related to probability of exposure calculated from the Landsat 2008-2010 composite image (x-axis). The median value and interquartile range of each group are reported here. A linear regression was fitted to all data points (not shown) with an equation of (lidar exposure) =1.1947(Landsat exposure)-0.2529. R^2=0.937.*

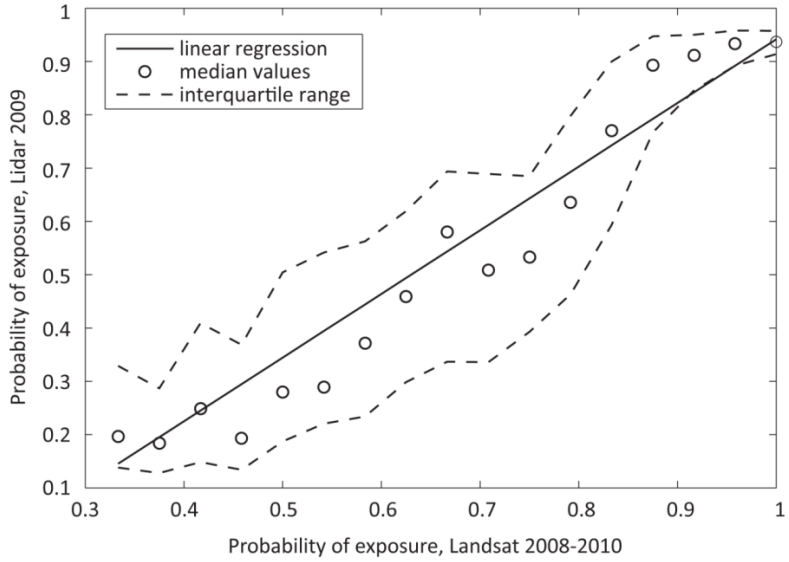

3.2.2. Topographic change over time

As can be seen in both the Landsat exposure probability and Landsat elevation maps (Fig. 10, 11), the topography of Pintail Island developed from a non-systematic arrangement of elevations (1999-2001) to a discrete levee and intra-island platform (2008-2010). Based on the distribution of vegetation types for the Wax Lake Delta from Carle et al. (Fig. 12c), the peaks in the elevation histogram for each time period were classified as “mudflat”, “low marsh” and “high marsh” (Fig. 12 a, b). Though the 2008-2010 histogram appears to have a fourth peak at 0.8 m (Fig. 12a), the peak does not appear in the Lidar 2009 elevation histogram (Fig. 12b), so is interpreted as being an artifact of the smaller number of points used to construct the Landsat histogram and lower resolution at the tail of the distribution, and not as a separate habitat zone. The elevation distribution histograms overall transition from one peak to three peaks (Fig. 13). In 1999-2001, the primary peak was at 0.41 m with small peaks at -0.5 and 0.8 m. In 2002-2004, the peaks were at -0.05, 0.36, and 0.82 m. In 2005-2007, the peaks were at -0.05, 0.26, and 0.82 m. In 2008-2010, the peak elevations were -0.05 m, 0.26, and 0.51 m. Over time, the total area classified as low marsh decreased and the high marsh and mudflat zones increased. Sites 1 and 2 transition from low marsh to high marsh by 2002-2004 (Fig. 14), with trees growing in around 2000-02 (Table 5). Site 3 transitions from low marsh to high marsh by 2008-2010, with trees establishing around 2008. Site 4 is low marsh just transitioning to high marsh in 2008-2010. Site 5 goes from mudflat to low marsh in 2005-2007, with establishing around 2010.

Figure 10: Exposure probability for 4 different time periods calculated from Landsat imagery. A) 1999-2001, n=17. B) 2002-2004, n=19. C) 2005-2007, n=19. D) 2008-2010, n=24.

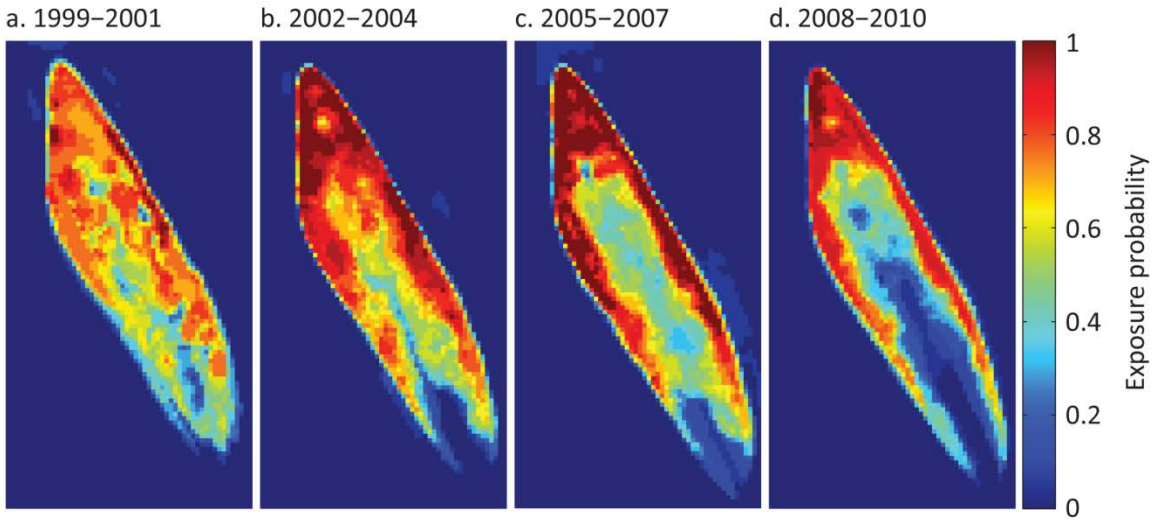

Figure 11: Elevation of Pintail Island approximated for four time periods, calculated using exposure probability (Fig. 9), the linear relationship between Lidar data and Landsat data exposure probability (Fig. 8), fitted surface water distribution (Fig. 4b), and water surface slope (Fig. 4c). a) 1999-2001. b) 2002-2004. c) 2005-2007. d) 2008-2010. Sediment core sampling sites 1-5 indicated by black circles.

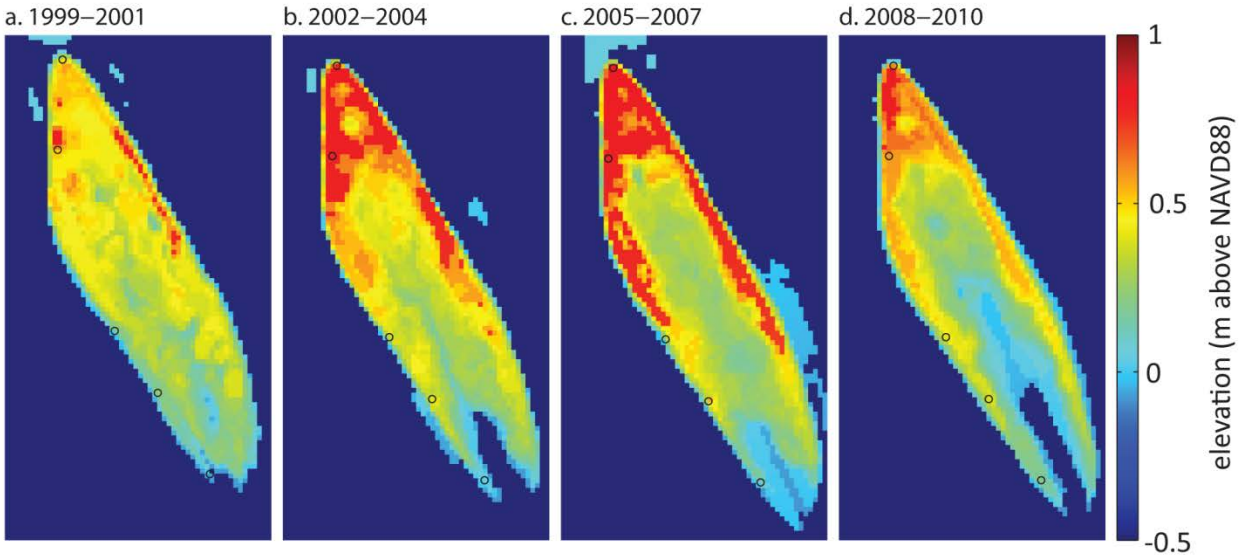

Figure 12: Habitat zonation from elevation and vegetation distributions. a) Elevation histogram from Landsat 2008-2010 results (n=1919). b) Elevation histogram from Lidar 2009 data (n=707,903). c) Vegetation distribution at the WLD after Carle et al. (2013). Dashed lines indicate interpreted habitat zones based on the Landsat 2008-2010 and Lidar 2009 histogram (Fig. 11d).

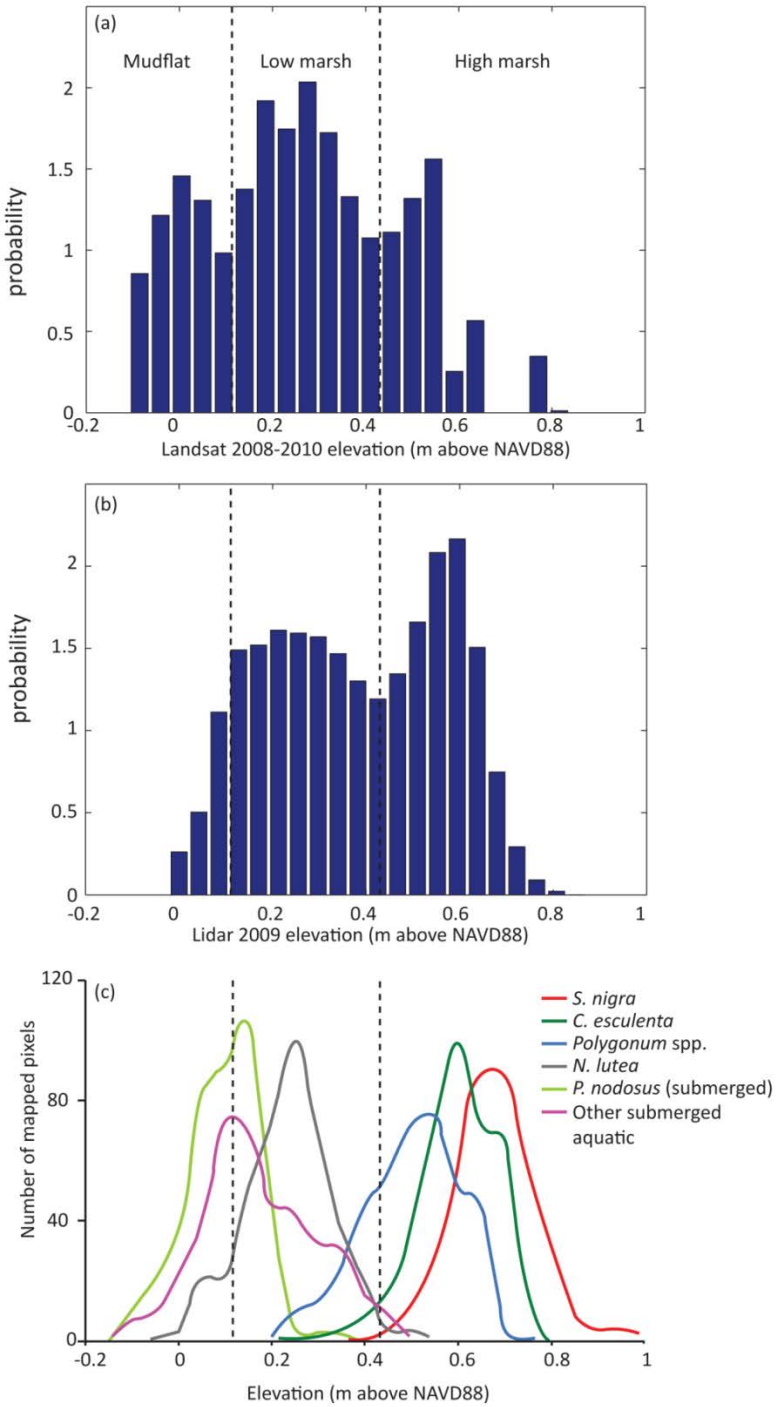

Figure 13: Histograms showing distribution of elevation for four time periods. a) 1999-2001, n=17. B) 2002-2004, n=19. C) 2005-2007, n=19. D) 2008-2010, n=24. Colors indicate divisions between peaks used to determine habitat zones. Orange=high marsh, green=low marsh, light blue=mudflat.

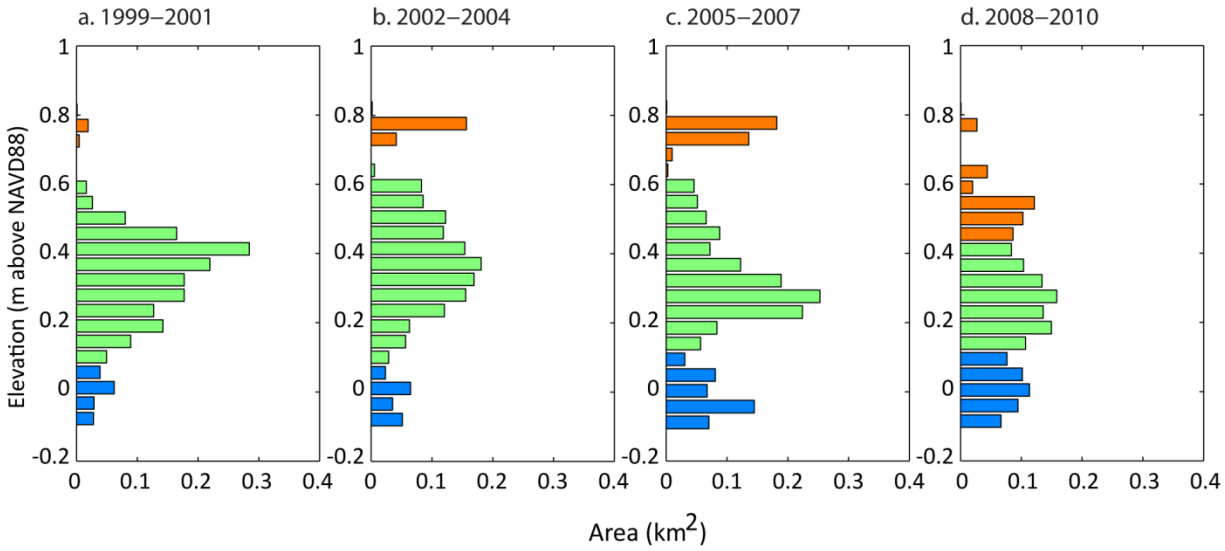

Figure 14: Island elevations grouped into habitat zones by peaks in histogram. Orange=high marsh, green=low marsh, light blue=mudflat, dark blue=open water. Red circles indicate location of 5 core sampling sites.

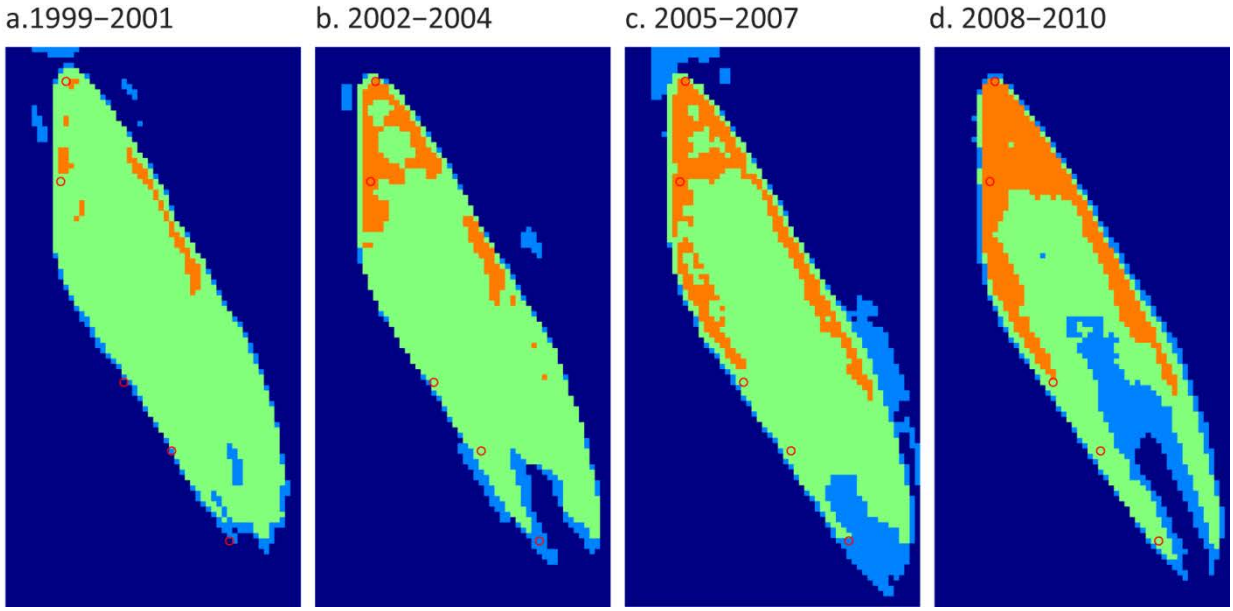

Table 5: S. nigra *ages from tree core data*

Site	median age (years)	age range (years)	n
1	12	12-13	4
2	10	8-11	6
3	5	5	1
4	no trees		
5	4	4	2

4. DISCUSSION

4.1. EVOLUTION OF ISLAND TOPOGRAPHY OVER TIME

The most notable change in the island topography over time was the organization and development of distinct platforms at the approximate elevations 0, 0.25, and 0.5 m above NAVD88 (Fig. 13). In contrast to the theoretical vegetation distribution as a function of elevation as described by Viparelli et al. (2011) (Fig. 2) which shows five distinct habitat groups, the observed vegetation distribution at the WLD can be grouped into two general vegetation types, high marsh and low marsh (Carle et al., 2013). Low marsh species such as *N. lutea* and *P. nodosus* are found at WLD at an elevation between 0 and 0.4 m, with peak *N. lutea* growth at approximately 0.25 m; similarly, high marsh vegetation *C. esculenta* and *S. nigra* are distributed between 0.4-1 m elevation, where peak C. esculenta growth occurs a 0.6 m according to Carle et al. (2013) (Fig. 12c). The platform at 0 m would be suitable only for submerged aquatic vegetation. Based on field observations, this area has little to no vegetation and consisted primarily of a mudflat. Overall, this vegetation grouping shows a close correspondence between elevation and vegetation distribution on Pintail Island.

The Landsat waterline method was successful in capturing the relative distribution of elevation over time, with a near 1:1 relationship between the Landsat 2008-2010 and Lidar 2009 probability of exposure data (Fig. 9). However, there were inherent uncertainties in the method, given that there are topographic features on the delta smaller than the available 30 m horizontal resolution. Calculating inundation frequencies assumed that the surface water slope remains consistent, and the water level distribution

around mean local water level remained the same throughout the delta and through time. This method also assumed that the delta had not significantly changed over each three year time period used; while this is likely untrue, a compromise was necessary to have a sufficient sample size for each group. Also, the method differentiating water from land (Otsu, 1979) would have identified dense stands of vegetation such as *N. lutea* as land even if they were in fact growing in water. Similarly, tree stands would be identified as land even if they were completely flooded beneath the canopy. For these reasons, the absolute elevations of the peaks identified in the elevation distribution histogram could vary in part due to error in the method rather than an actual shift in dominant elevation. Nevertheless, the reconstruction of historical island elevation changes and the relative distribution of elevations and organization into distinct platforms is a significant result.

Multiple modeling studies have described tidal marshes as developing equilibrium elevations as a result of negative feedbacks creating alternative stable states which are resistant to perturbation (Marani et al., 2013; Da Lio et al., 2013; D'Alpaos et al., 2012). To achieve these multiple stable elevations, plant communities must exhibit a high degree of specialization with peak productivity at different elevations, and accretion rate must be a function of plant productivity. Based on modeling work done on salt marshes, it has been proposed that the signature of this process is multiple peaks in the elevation histogram which correspond with vegetation type (Marani et al., 2013). The specialized vegetation (Fig. 12c), emergence of distinct elevation groupings (Figs. 12, 14), abrupt transitions between platforms, and close correlation with vegetation distribution (Fig. 12) strongly suggests that alternative stable state theory applies to this location. This is a

novel finding because such theory, largely recently developed for salt marshes, has not previously been tested for a rapidly prograding delta environment.

4.2. EVIDENCE IN THE SEDIMENT RECORD FOR VEGETATIVE INFLUENCE ON TOPOGRAPHIC CHANGE

Generally, alternative stable state theory assumes a positive correlation between biomass and soil accumulation such that increased biomass is positively correlated to soil organic matter accumulation (Marani et al., 2013; Da Lio et al., 2013; Mudd et al., 2009), mineral sedimentation (Morris et al., 2002), or both (D'Alpaos et al., 2012). Vegetation has been observed to influence topographic change in a tidal environment via several mechanisms, including organic matter accumulation, mineral sediment accumulation through water velocity attenuation, and erosion reduction by increased cohesion (Lorenzo-Trueba et al., 2012; Leonard and Luther, 1995; Christiansen et al., 2000). If these positive effects on elevation growth are balanced by negative factors like erosion and compaction, the combined effect would be a negative feedback regulating a stable elevation. The evidence from this study (Figs. 12, 13) suggests these negative feedbacks are occurring at the WLD.

4.2.1 Organic sediment accumulation

In systems with low mineral sediment inputs like many salt marshes, organic matter is the primary driver of elevation change (Marani et al., 2013; Mudd et al., 2009; Nyman et al., 2006; Kirwan and Guntenspergen, 2012; Bricker-Urso et al., 1989). Organic matter deposition is positively, and mineral sediment deposition negatively,

correlated to elevation. If organic matter were the sole driver of elevation growth, as elevation increases with added organic matter, less and less mineral sediment would be deposited, so organic matter would need to account for most of the total growth. Although there was some clear organic matter contribution to the vertical growth of Pintail Island (Fig. 7), it was not sufficient to account for all the elevation change required to achieve the differentiation from low marsh to high marsh indicated by the remote sensing record. The mean total vertical contribution made by organic matter ranges from a minimum of 1.4% of core length (Site 5H) to a maximum of 10.3 % of core length (Site 2T), corresponding to approximately 9 cm of elevation gain. In contrast, the difference in elevation between the high and low marsh of Pintail Island is approximately 25 cm (Fig. 13), so the differentiation of elevation exhibited could not be entirely a function of organic matter deposition. However, depending on the degree of specialization, a small elevation difference can change biomass production significantly (Morris, 2006), so a threshold elevation could be achieved by a small amount of elevation growth contributed by organic matter, for example by making the local elevation more favorable to a species that is better at trapping sediment. This could explain why there is substantially less organic matter in cores from Site 5 than the other 4 sites (Fig. 6a, d), especially 5H. Even Site 4H, only 15 cm higher, has approximately twice as much total organic matter (Fig. 7), suggesting a strong positive feedback occurred between organic matter production and elevation near or above MLWL causing rapid accumulation, with further elevation growth by both organic and mineral sedimentation thereafter.

.

Though the vegetation communities at the WLD have specific elevation ranges (Fig. 12c), there did not appear to be a strong differentiation in organic matter accumulation as a function of plant productivity. If organic matter inputs were the primary mechanism of altering elevation, the sediment cores would likely exhibit a higher degree of specialization in soil organic matter profiles between species and across elevations. Site 3 was the only site to have significantly different total organic matter contributions between 3H and 3T (Fig. 7). Similarly, cores taken within *C. esculenta* at Sites 1H-3H had very similar organic matter profiles (Fig. 6d) and total organic matter contributions (Fig. 7) across a range of elevations from 0.75 m (Site 1) to 0.47 m (Site 3). In particular, Site 3 at 0.47 m was on the low end of the ideal elevation range for *C. esculenta* (Fig. 2, 12c), and would be expected to be less productive and therefore contribute less organic matter to the soil. The lack of variation indicates that organic matter is likely not the mechanism driving the organization of island topography into platforms. However, plant productivity indicators were not quantified in this study so it is possible that the full range of plant productivity was not captured accurately. For example, it became apparent in the field that microtopography exists such that at these sites the herbaceous plots can be lower from 0- 5 cm (Sites 1-3) to 10 cm lower (Site 5) than the tree plots. This effect might be compounded at lower sites as the difference in inundation frequency would be larger.

4.2.2. Mineral sediment accumulation rates

The rate of mineral sediment accumulation is generally expected to decrease as a function of elevation due to decreased flooding frequency, less sediment delivered in the event of a flood, and overall finer sediment delivered which would tend to deposit over a larger area (James, 1985; Pizzuto, 1987; Leonard and Luther, 1995; Cahoon and Reed, 1995).The predicted maximum height would be approached at approximately the mean high water level (D'Alpaos, 2011). Cahoon et al. (2011) used marker horizons in a similar environment in the Mississippi River delta to confirm that accretion rates decreased with increased elevation. We can place some bounds on the overall average rate of sediment supply to the WLD based on the initial elevation of Atchafalaya Bay at approximately -2 m above NAVD88 (Shaw et al., 2013) relative to the total deposition required since the inception of the WLD to raise Pintail Island to its current elevation at 0.2-0.75 m above NAVD88 (Fig. 8a). Depending on the total accretion (2.2-2.75 m) and assumed length of time deposition has been occurring (40-60 years), the average deposition on Pintail Island could range from a minimum of 3.7 cm/yr to a maximum of 6.9 cm/yr. However, much higher rates might be expected initially, as lower elevations would be flooded more frequently; repeated bathymetric surveys in the subaqueous delta front show that flood events can deposit up to 50 cm of sediment at a time (Shaw et al., 2013). Lower rates might be expected as elevation increased to near high water level. This simple, time-averaged model also does not take into account the influence of large discrete depositional events, which appear as peaks in the Pb-210 accumulation rates and grain size profiles, and could explain the overall non-monotonic trends in these data (Fig.

5). Event driven deposition has been observed in other deltaic studies (Esposito et al., 2013; Shaw et al., 2013).

In contrast to the expected pattern of sedimentation, mineral sediment accumulation rates at Sites 1-4 all showed a significant increase in sedimentation with increasing elevation (decreasing depth) in the cores, while Sites 5H and 5T did not show a significant trend with depth (Table 4). Modeling of salt marshes has suggested that an accelerated growth rate of marsh elevation near MLWL is indicative of vegetation exerting an influence on the accretion rate, though in the sediment limited environment of many salt marshes, this has been attributed primarily to organic matter deposition (D'Alpaos, 2011). This increased mineral sedimentation is consistent with previous findings that water velocity and turbulence are inversely related to stem density (Leonard and Luther, 1995; Nepf, 2012; Christiansen et al., 2000; Gleason et al., 1979). In two out of three sites with two plant species above MLWL (Sites 1-3), the accumulation rates in the herbaceous vegetation plot was higher than rates in the tree plots (Table 4), suggesting that the relatively higher stem density of the *C. esculenta* may be having a stronger effect on sedimentation rates. The overall higher variability in mineral accumulation rates across the herbaceous sites (Fig. 6f) in comparison to the tree sites (Fig. 6c) is consistent with expected differences in productivity given the range of species and elevations captured by these sampling sites, and therefore could be a factor in driving the alternative stable state process.

Though the consistent correlation between accumulation rates and elevation across Sites 1-4 lends confidence to this interpretation, uncertainty associated with the

correction for core compression could have had an effect on the Pb-210 dating analysis due to its dependence on accurate depths and densities. Also, the Pb-210 CRS dating model used to find accumulation rates was based on the assumption that the excess Pb-210 was supplied to the sediment surface at a constant rate throughout core. If the rate of supply actually decreased, the apparent sediment accumulation rate would go up over time, which could theoretically have contributed to the observed higher accretion rates at shallower depths in the cores. The lack of a significant trend at Site 5 could indicate steady growth, or could be the result of lower clay content for ^{210}Pb to adsorb to, causing low activities which are hard to measure accurately.

4.2.3. Grain size patterns

The observed negative correlation between elevation and median grain size at the WLD is consistent with the expected abiotic morphodynamics of delta island levee and mouth bar deposition in which higher elevations experience fewer inundation and deposition events, less and finer sediment delivered from higher in the water column, and lower shear stresses associated with lower water depths (Allen, 1992; Woolnough et al., 1995; James, 1985; Pizzuto, 1987).Variation around this general trend is also expected, as fluctuating water and sediment levels create different depositional regimes throughout the year, resulting in interbedded sands and muds (Esposito et al., 2013). This fining upward trend is also consistent with the observed higher total sedimentation rates with decreasing depth. If vegetation is in fact increasing mineral sedimentation by slowing water velocity, this would also tend to decrease the average grain size of the deposited sediment (Bos et

al., 2007; Yang et al., 2008; Yang, 1998; van Hulzen et al., 2007). However, since vegetation would only enhance a fining upward trend that can also be attributed to abiotic factors, evidence in the core record is insufficient to verify this vegetation- dominated mechanism. The significantly lower median grain size at herbaceous sites 1H and 3H compared to tree sites 1T and 1H suggests that the higher stem density of the herbaceous vegetation could be accelerating this fining upward trend, but there is not a clear pattern across all sites.

Some variability in observed grain size distributions and profiles was also likely a result of spatial heterogeneity and microtopography, such as the abrupt sandy layer at Sites 1T and 2T at about 40 cm depth, which did not appear at Sites 1H and 2H. Historical photos show that the distribution of tree stands at Site 1 and 2 appears to be controlled by the location of old channels that cut through the levee, and sites presently dominated by herbaceous vegetation were previously channels. In the event of a large flood and corresponding sandy deposit, it is possible that deposition either did not occur or was not preserved in these channels(now 1H and 2H) but was preserved on adjacent lands that were higher at the time (now 1T and 2T). Therefore, local-scale historical morphodynamics not only partly explain the sedimentation recorded in the cores, but also likely some of the present ecological arrangement of the island vegetation community.

In general, clay and silt deposits increase cohesion, requiring higher velocities to entrain than their size alone would suggest, though low velocities are typically required for deposition. Overall, the median grain size of these core profiles frequently falls below the 62 micron threshold between sand and silt, indicating the presence of a substantial

amount of silt and clay in the shallow subsurface. The observed upward fining of mineral sediment should produce increased cohesion on the island top as a result of the increasing dominance by muddy material. Though unclear how much this fining upward is the result of vegetative growth, this increased cohesion could potentially have a significant effect on mouth bars and levee dynamics that control island initiation and overall delta geometry (Edmonds and Slingerland, 2009; Hoyal and Sheets, 2009; Rowland et al., 2010).

.

5. CONCLUSION

The evidence from Pintail Island further confirms that Wax Lake Delta island development is consistent with previous delta studies; however, the specific patterns of organic vs. mineral sediment accumulation, accumulation rates over time and space, and relations to island elevation and vegetation zonation provide new insights into possible feedbacks between ecologic succession and geomorphic processes.

The self-organization of island elevations into distinct platforms coincident with vegetation distribution suggests that alternative stable state theory applies WLD ecogeomorphological dynamics. Based on the evidence from the core and remote sensing analyses of Pintail Island, it seems likely that the spatial arrangement of the levee and intra-island platform, initially formed by abiotic processes, is altered by levee vegetation sieving more and finer sediment out of flowing water when flooded, creating a higher and more cohesive levee system and reducing sediment availability towards the interior of the island.

This study found some contribution to vertical island growth by organic matter, but not a sufficient amount to account for all the elevation change required to achieve the differentiation from low marsh to high marsh deduced from the time-lapse Landsat imagery analysis. Mineral sediment accumulation rates suggested that elevation growth was accelerating or holding steady over time, in contrast to theory suggesting rates should slow with increasing elevation. At two of the five field sites, this effect appeared stronger among the more dense stems of herbaceous vegetation than among the more sparse stems of mature trees. Mineral sedimentation appeared to prevail over organic sedimentation as

the main factor for elevation change along the levee on Pintail Island, in contrast to current models sedimentation in somewhat analogous salt marsh systems.

If enhanced mineral sedimentation within levee vegetation indeed restricts the ability for sediment to traverse the levee and reach the island interior, then the levee should be more resilient than the interior island region to sea level rise or minor changes in sediment supply. Overall, the existence of multiple stable elevations in a delta such as the WLD has implications for the ecology and stability of coastal marshes. In particular, the issue of land loss in coastal management may benefit from a focus on stable or unstable marsh conditions in low gradient tidal systems where it is difficult to define the transition from land to water.

6. REFERENCES

Aalto, R., and Nittrouer, C.A., 2012, 210Pb geochronology of flood events in large tropical river systems: Philosophical Transactions of the Royal Society A: Mathematical, Physical and Engineering Sciences, v. 370, p. 2040–2074, doi: 10.1098/rsta.2011.0607.

Allen, J.R.L., 1992, Large-scale textural patterns and sedimentary processes on tidal salt marshes in the Severn Estuary, southwest Britain: Sedimentary Geology, v. 81, p. 299–318, doi: 10.1016/0037-0738(92)90077-5.

Allen, Y.C., Couvillion, B.R., and Barras, J.A., 2011, Using Multitemporal Remote Sensing Imagery and Inundation Measures to Improve Land Change Estimates in Coastal Wetlands: Estuaries and Coasts, v. 35, p. 190–200, doi: 10.1007/s12237-011-9437-z.

Allison, M.A., Demas, C.R., Ebersole, B.A., Kleiss, B.A., Little, C.D., Meselhe, E.A., Powell, N.J., Pratt, T.C., and Vosburg, B.M., 2012, A water and sediment budget for the lower Mississippi–Atchafalaya River in flood years 2008–2010: Implications for sediment discharge to the oceans and coastal restoration in Louisiana: Journal of Hydrology, v. 432-433, p. 84–97, doi: 10.1016/j.jhydrol.2012.02.020.

Appleby, P.G., 2008, Three decades of dating recent sediments by fallout radionuclides: a review: The Holocene, v. 18, p. 83–93, doi: 10.1177/0959683607085598.

Appleby, P.G., and Oldfield, F., 1983, The assessment of 210Pb data from sites with varying sediment accumulation rates: Hydrobiologia, v. 103, p. 29–35, doi: 10.1007/BF00028424.

Appleby, P.G., and Oldfield, F., 1978, The calculation of lead-210 dates assuming a constant rate of supply of unsupported 210Pb to the sediment: CATENA, v. 5, p. 1–8, doi: 10.1016/S0341-8162(78)80002-2.

Bos, A.R., Bouma, T.J., de Kort, G.L.J., and van Katwijk, M.M., 2007, Ecosystem engineering by annual intertidal seagrass beds: Sediment accretion and modification: Estuarine, Coastal and Shelf Science, v. 74, p. 344–348, doi: 10.1016/j.ecss.2007.04.006.

Bricker-Urso, S., Nixon, S.W., Cochran, J.K., Hirschberg, D.J., and Hunt, C., 1989, Accretion rates and sediment accumulation in Rhode Island salt marshes: Estuaries, v. 12, p. 300–317, doi: 10.2307/1351908.

Cahoon, D.R., and Reed, D.J., 1995, Relationships among marsh surface topography,

hydroperiod, and soil accretion in a deteriorating Louisiana salt marsh: Journal of Coastal Research, v. 11, p. 357–369.

Cahoon, D.R., White, D.A., and Lynch, J.C., 2011, Sediment infilling and wetland formation dynamics in an active crevasse splay of the Mississippi River delta: Geomorphology, v. 131, p. 57–68, doi: 10.1016/j.geomorph.2010.12.002.

Carle, M.V., Sasser, C.E., and Roberts, H.H., 2013, Accretion and Vegetation Community Change in the Wax Lake Delta Following the Historic 2011 Mississippi River Flood: Journal of Coastal Research,.

Christiansen, T., Wiberg, P.L., and Milligan, T.G., 2000, Flow and Sediment Transport on a Tidal Salt Marsh Surface: Estuarine, Coastal and Shelf Science, v. 50, p. 315–331, doi: 10.1006/ecss.2000.0548.

Craft, C., 2007, Freshwater input structures soil properties, vertical accretion, and nutrient accumulation of Georgia and US tidal marshes: Limnology and oceanography,, p. 1220–1230.

D'Alpaos, A., 2011, The mutual influence of biotic and abiotic components on the long-term ecomorphodynamic evolution of salt-marsh ecosystems: Geomorphology, v. 126, p. 269–278, doi: 10.1016/j.geomorph.2010.04.027.

D'Alpaos, A., Da Lio, C., and Marani, M., 2012, Biogeomorphology of tidal landforms: physical and biological processes shaping the tidal landscape: Ecohydrology, v. 5, p. 550–562, doi: 10.1002/eco.279.

Darke, A.K., and Megonigal, J.P., 2003, Control of sediment deposition rates in two mid-Atlantic Coast tidal freshwater wetlands: Estuarine, Coastal and Shelf Science, v. 57, p. 255–268, doi: 10.1016/S0272-7714(02)00353-0.

Edmonds, D.A., and Slingerland, R.L., 2007, Mechanics of river mouth bar formation: Implications for the morphodynamics of delta distributary networks: Journal of Geophysical Research, v. 112, p. F02034, doi: 10.1029/2006JF000574.

Edmonds, D.A., and Slingerland, R.L., 2009, Significant effect of sediment cohesion on delta morphology: Nature Geoscience, v. 3, p. 105–109, doi: 10.1038/ngeo730.

Esposito, C.R., Georgiou, I.Y., and Kolker, A.S., 2013, Hydrodynamic and geomorphic controls on mouth bar evolution: Geophysical Research Letters, v. 40, p. 1540–1545, doi: 10.1002/grl.50333.

Fagherazzi, S., Kirwan, M.L., Mudd, S.M., Guntenspergen, G.R., Temmerman, S., D'Alpaos, A., van de Koppel, J., Rybczyk, J.M., Reyes, E., and Craft, C., 2012, Numerical models of salt marsh evolution: Ecological, geomorphic, and climatic

factors: Reviews of Geophysics, v. 50, p. RG1002.

Gedan, K.B., Kirwan, M.L., Wolanski, E., Barbier, E.B., and Silliman, B.R., 2011, The present and future role of coastal wetland vegetation in protecting shorelines: answering recent challenges to the paradigm: Climatic Change, v. 106, p. 7–29.

Geleynse, N., Hiatt, M., Sangi, H., and Passalacqua, P. Identifying environmental controls on the shoreline of a natural river delta: in review,.

Geleynse, N., Voller, V.R., Paola, C., and Ganti, V., 2012, Characterization of river delta shorelines: Geophysical Research Letters, v. 39, p. n/a–n/a, doi: 10.1029/2012GL052845.

Gleason, M.L., Elmer, D.A., Pien, N.C., and Fisher, J.S., 1979, Effects of stem density upon sediment retention by salt marsh cord grass, Spartina alterniflora loisel: Estuaries, v. 2, p. 271–273, doi: 10.2307/1351574.

Hargis, T.G., and Twilley, R.R., 1994, Improved coring device for measuring soil bulk density in a Louisiana deltaic marsh: Journal of Sedimentary Research, v. 64, p. 681–683.

He, Q., and Walling, D.E., 1996, USE OF FALLOUT Pb-210 MEASUREMENTS TO INVESTIGATE LONGER-TERM RATES AND PATTERNS OF OVERBANK SEDIMENT DEPOSITION ON THE FLOODPLAINS OF LOWLAND RIVERS: Earth Surface Processes and Landforms, v. 21, p. 141–154, doi: 10.1002/(SICI)1096-9837(199602)21:2<141::AID-ESP572>3.0.CO;2-9.

Van Heerden, I., and Roberts, H., 1988, Facies development of Atchafalaya Delta, Louisiana: A modern bayhead delta: The American Association of Petroleum Geologist Bulletin, v. 72, p. 439–453.

Hiatt, M., Wagner, R.W., Geleynse, N., Minton, B., and Passalacqua, P. Network flow partitioning, island hydrodynamics, and environmental controls at Wax Lake Delta, Louisiana: in review,.

Hoyal, D.C.J.D., and Sheets, B.A., 2009, Morphodynamic evolution of experimental cohesive deltas: Journal of Geophysical Research, v. 114, p. F02009, doi: 10.1029/2007JF000882.

Van Hulzen, J.B., van Soelen, J., and Bouma, T.J., 2007, Morphological variation and habitat modification are strongly correlated for the autogenic ecosystem engineerSpartina anglica (common cordgrass): Estuaries and Coasts, v. 30, p. 3–11, doi: 10.1007/BF02782962.

James, C.S., 1985, Sediment transfer to overbank sections: Journal of Hydraulic

Research, v. 23, p. 435–452, doi: 10.1080/00221688509499337.

Johnson, W. b., Sasser, C. e., and Gosselink, J. g., 1985, Succession of Vegetation in an Evolving River Delta, Atchafalaya Bay, Louisiana: Journal of Ecology, v. 73, p. 973.

Van Katwijk, M.M., Bos, A.R., Hermus, D.C.R., and Suykerbuyk, W., 2010, Sediment modification by seagrass beds: Muddification and sandification induced by plant cover and environmental conditions: Estuarine, Coastal and Shelf Science, v. 89, p. 175–181, doi: 10.1016/j.ecss.2010.06.008.

Kesel, R.H., 2003, Human modifications to the sediment regime of the Lower Mississippi River flood plain: Geomorphology, v. 56, p. 325–334, doi: 10.1016/S0169-555X(03)00159-4.

Kim, W., Dai, A., Muto, T., and Parker, G., 2009, Delta progradation driven by an advancing sediment source: Coupled theory and experiment describing the evolution of elongated deltas: Water Resources Research, v. 45, p. W06428, doi: 10.1029/2008WR007382.

Kirwan, M.L., and Guntenspergen, G.R., 2012, Feedbacks between inundation, root production, and shoot growth in a rapidly submerging brackish marsh: Journal of Ecology,.

Kirwan, M.L., and Murray, A.B., 2007, A coupled geomorphic and ecological model of tidal marsh evolution: Proceedings of the National Academy of Sciences, v. 104, p. 6118–6122.

Leonard, L.A., and Luther, M.E., 1995, Flow Hydrodynamics in Tidal Marsh Canopies: Limnology and Oceanography, v. 40, p. 1474–1484.

Da Lio, C., D'Alpaos, A., and Marani, M., 2013, The secret gardener: vegetation and the emergence of biogeomorphic patterns in tidal environments: Philosophical Transactions of the Royal Society A: Mathematical, Physical and Engineering Sciences, v. 371, p. 20120367, doi: 10.1098/rsta.2012.0367.

Lorenzo-Trueba, J., Voller, V.R., Paola, C., Twilley, R.R., and Bevington, A.E., 2012, Exploring the role of organic matter accumulation on delta evolution: Journal of Geophysical Research, v. 117, p. F00A02, doi: 10.1029/2012JF002339.

Marani, M., D'Alpaos, A., Lanzoni, S., Carniello, L., and Rinaldo, A., 2010, The importance of being coupled: Stable states and catastrophic shifts in tidal biomorphodynamics: Journal of Geophysical Research: Earth Surface, v. 115, p. n/a–n/a, doi: 10.1029/2009JF001600.

Marani, M., Da Lio, C., and D'Alpaos, A., 2013, Vegetation engineers marsh morphology through multiple competing stable states: Proceedings of the National Academy of Sciences of the United States of America, v. 110, p. 3259–3263, doi: 10.1073/pnas.1218327110.

Mason, D.C., Scott, T.R., and Dance, S.L., 2010, Remote sensing of intertidal morphological change in Morecambe Bay, U.K., between 1991 and 2007: Estuarine, Coastal and Shelf Science, v. 87, p. 487–496, doi: 10.1016/j.ecss.2010.01.015.

McGranahan, G., Balk, D., and Anderson, B., 2007, The rising tide: assessing the risks of climate change and human settlements in low elevation coastal zones: Environment and Urbanization, v. 19, p. 17–37, doi: 10.1177/0956247807076960.

Micheli, E.R., and Kirchner, J.W., 2002, Effects of wet meadow riparian vegetation on streambank erosion. 2. Measurements of vegetated bank strength and consequences for failure mechanics: Earth Surface Processes and Landforms, v. 27, p. 687–697.

Morris, J.T., 2006, Competition among marsh macrophytes by means of geomorphological displacement in the intertidal zone: Estuarine, Coastal and Shelf Science, v. 69, p. 395–402, doi: 10.1016/j.ecss.2006.05.025.

Morris, J.T., Sundareshwar, P.V., Nietch, C.T., Kjerfve, B., and Cahoon, D.R., 2002, Responses of coastal wetlands to rising sea level: Ecology, v. 83, p. 2869–2877.

Mudd, S.M., Howell, S.M., and Morris, J.T., 2009, Impact of dynamic feedbacks between sedimentation, sea-level rise, and biomass production on near-surface marsh stratigraphy and carbon accumulation: Estuarine, Coastal and Shelf Science, v. 82, p. 377–389.

NASA, 2010, NASA Landsat Program: Landsat Path 23, Rows 39 and 40, 1999-2010: USGS http://earthexplorer.usgs.gov,.

NCALM, 2009, Lidar Dataset, Wax Lake Delta: National Center for Airborne Laser Mapping. Houston, TX., v. Jan. 14, 2009.

Nepf, H.M., 2012, Hydrodynamics of vegetated channels: Journal of Hydraulic Research, v. 50, p. 262–279, doi: 10.1080/00221686.2012.696559.

Neubauer, S.C., 2008, Contributions of mineral and organic components to tidal freshwater marsh accretion: Estuarine, Coastal and Shelf Science, v. 78, p. 78–88, doi: 10.1016/j.ecss.2007.11.011.

Neves, P.A., Lima Ferreira, P.A., Bícego, M.C., and Figueira, R.C.L., 2014,

Radioanalytical assessment of sedimentation rates in Guajará Bay (Amazon Estuary, N Brazil): a study with unsupported 210Pb and 137Cs modeling: Journal of Radioanalytical and Nuclear Chemistry, v. 299, p. 407–414, doi: 10.1007/s10967-013-2834-y.

NOAA, 2013, National Oceanographic and Atmospheric Administration: Tides and Currents Harmonic Constituents for 8764227, Lawma, Amerada Pass, Louisiana: http://tidesandcurrents.noaa.gov/,.

NRCS, 2004, Soil Survey Laboratory Methods Manual: U.S. Department of Agriculture, Natural Resources Conservation ServiceSoil Survey Investigations Report, v. 42.

Nyman, J.A., Walters, R.J., Delaune, R.D., and Patrick Jr., W.H., 2006, Marsh vertical accretion via vegetative growth: Estuarine, Coastal and Shelf Science, v. 69, p. 370–380, doi: 10.1016/j.ecss.2006.05.041.

Orton, G.J., and Reading, H.G., 1993, Variability of deltaic processes in terms of sediment supply, with particular emphasis on grain size: Sedimentology, v. 40, p. 475–512, doi: 10.1111/j.1365-3091.1993.tb01347.x.

Otsu, N., 1979, A Threshold Selection Method from Gray-Level Histograms: IEEE Transactions on Systems, Man and Cybernetics, v. 9, p. 62–66, doi: 10.1109/TSMC.1979.4310076.

Palinkas, C.M., Engelhardt, K.A.M., and Cadol, D., 2013, Evaluating physical and biological influences on sedimentation in a tidal freshwater marsh with 7Be: Estuarine, Coastal and Shelf Science, v. 129, p. 152–161, doi: 10.1016/j.ecss.2013.05.022.

Palmer, M.R., Nepf, H.M., Pettersson, T.J.R., and Ackerman, J.D., 2004, Observations of Particle Capture on a Cylindrical Collector: Implications for Particle Accumulation and Removal in Aquatic Systems: Limnology and Oceanography, v. 49, p. 76–85.

Paola, C., Twilley, R.R., Edmonds, D.A., Kim, W., Mohrig, D., Parker, G., Viparelli, E., and Voller, V.R., 2011, Natural Processes in Delta Restoration: Application to the Mississippi Delta: Annual Review of Marine Science, v. 3, p. 67–91, doi: 10.1146/annurev-marine-120709-142856.

Parker, G., and Sequeiros, O., 2006, Large scale river morphodynamics: Application to the Mississippi delta, *in* River Flow 2006: Proceedings of the International Conference on Fluvial Hydraulics, Lisbon, Portugal, 6–8 September 2006, p. 3–11.

Pasternack, G., and Brush, G., 2001, Seasonal Variations in Sedimentation and Organic Content in Five Plant Associations on a Chesapeake Bay Tidal Freshwater Delta: Estuarine, Coastal and Shelf Science, v. 53, p. 93–106, doi: 10.1006/ecss.2001.0791.

Pizzuto, J.E., 1987, Sediment diffusion during overbank flows: Sedimentology, v. 34, p. 301–317, doi: 10.1111/j.1365-3091.1987.tb00779.x.

Pollen-Bankhead, N., and Simon, A., 2010, Hydrologic and hydraulic effects of riparian root networks on streambank stability: Is mechanical root-reinforcement the whole story?: Geomorphology, v. 116, p. 353–362, doi: 10.1016/j.geomorph.2009.11.013.

Roberts, H.H., 1997, Dynamic changes of the Holocene Mississippi River delta plain: the delta cycle: Journal of Coastal Research,, p. 605–627.

Rosen, T., and Xu, Y.J., 2013, Recent decadal growth of the Atchafalaya River Delta complex: Effects of variable riverine sediment input and vegetation succession: Geomorphology, v. 194, p. 108–120, doi: 10.1016/j.geomorph.2013.04.020.

Rouse, L.J., Roberts, H.H., and Cunningham, R.H.W., 1978, Satellite observation of the subaerial growth of the Atchafalaya Delta, Louisiana: Geology, v. 6, p. 405–408, doi: 10.1130/0091-7613(1978)6<405:SOOTSG>2.0.CO;2.

Rowland, J.C., Dietrich, W.E., and Stacey, M.T., 2010, Morphodynamics of subaqueous levee formation: Insights into river mouth morphologies arising from experiments: Journal of Geophysical Research: Earth Surface, v. 115, p. n/a–n/a, doi: 10.1029/2010JF001684.

Rühlmann, J., Körschens, M., and Graefe, J., 2006, A new approach to calculate the particle density of soils considering properties of the soil organic matter and the mineral matrix: Geoderma, v. 130, p. 272–283, doi: 10.1016/j.geoderma.2005.01.024.

Ryu, J.-H., Kim, C.-H., Lee, Y.-K., Won, J.-S., Chun, S.-S., and Lee, S., 2008, Detecting the intertidal morphologic change using satellite data: Estuarine, Coastal and Shelf Science, v. 78, p. 623–632, doi: 10.1016/j.ecss.2008.01.020.

Shaffer, G.P., Sasser, C.E., Gosselink, J.G., and Rejmanek, M., 1992, Vegetation dynamics in the emerging Atchafalaya Delta, Louisiana, USA: Journal of Ecology, v. 80, p. 677–687, doi: 10.2307/2260859.

Shaw, J.B., Mohrig, D., and Whitman, S.K., 2013, The morphology and evolution of channels on the Wax Lake Delta, Louisiana, USA: Journal of Geophysical

Research: Earth Surface, v. 118, p. 1562–1584, doi: 10.1002/jgrf.20123.

Simon, A., and Collison, A.J.C., 2002, Quantifying the mechanical and hydrologic effects of riparian vegetation on streambank stability: Earth Surface Processes and Landforms, v. 27, p. 527–546, doi: 10.1002/esp.325.

Stoddart, D.R., Reed, D.J., and French, J.R., 1989, Understanding salt-marsh accretion, Scolt Head Island, Norfolk, England: Estuaries, v. 12, p. 228–236, doi: 10.2307/1351902.

Stokes, M., and Smiley, T., 1968, An introduction to tree-ring dating: Chicago :, University of Chicago Press.

Temmerman, S., Bouma, T.J., Koppel, J.V. de, Wal, D.V. der, Vries, M.B.D., and Herman, P.M.J., 2007, Vegetation causes channel erosion in a tidal landscape: Geology, v. 35, p. 631–634, doi: 10.1130/G23502A.1.

U.S. Geological Survey, 2014, National Water Information System data available on the World Wide Web (Water Data for the Nation):.

Vandenbruwaene, W., Temmerman, S., Bouma, T.J., Klaassen, P.C., de Vries, M.B., Callaghan, D.P., van Steeg, P., Dekker, F., van Duren, L.A., Martini, E., Balke, T., Biermans, G., Schoelynck, J., and Meire, P., 2011, Flow interaction with dynamic vegetation patches: Implications for biogeomorphic evolution of a tidal landscape: Journal of Geophysical Research, v. 116, doi: 10.1029/2010JF001788.

Viparelli, E., Shaw, J., Bevington, A., Meselhe, E., Holm, G.O., Mohrig, D., Twilley, R., and Parker, G., 2011, Inundation Model as an Aid for Predicting Ecological Succession on Newly-Created Deltaic Land Associated with Mississippi River Diversions: Application to the Wax Lake Delta, *in* World Environmental and Water Resources Congress 2011@ sBearing Knowledge for Sustainability, p. 2340–2349.

Wellner, R., Beaubouef, R., Van Wagoner, J., Roberts, H., and Sun, T., 2005, Jet-plume depositional bodies—the primary building blocks of Wax Lake Delta:.

White, D.A., 1993, Vascular plant community development on mudflats in the Mississippi River delta, Louisiana, USA: Aquatic Botany, v. 45, p. 171–194, doi: 10.1016/0304-3770(93)90020-W.

Woolnough, S.J., Allen, J.R.L., and Wood, W.L., 1995, An exploratory numerical model of sediment deposition over tidal salt marshes: Estuarine, Coastal and Shelf Science, v. 41, p. 515–543, doi: 10.1016/0272-7714(95)90025-X.

Wright, L.D., and Coleman, J.M., 1974, Mississippi River mouth processes: effluent

dynamics and morphologic development: The Journal of Geology,, p. 751–778.

Yang, S.L., 1998, The Role ofScirpusMarsh in Attenuation of Hydrodynamics and Retention of Fine Sediment in the Yangtze Estuary: Estuarine, Coastal and Shelf Science, v. 47, p. 227–233, doi: 10.1006/ecss.1998.0348.

Yang, S.L., Li, H., Ysebaert, T., Bouma, T.J., Zhang, W.X., Wang, Y.Y., Li, P., Li, M., and Ding, P.X., 2008, Spatial and temporal variations in sediment grain size in tidal wetlands, Yangtze Delta: On the role of physical and biotic controls: Estuarine, Coastal and Shelf Science, v. 77, p. 657–671, doi: 10.1016/j.ecss.2007.10.024.

Zobeck, T.M., 2004, Rapid soil particle size analyses using laser diffraction: Applied engineering in agriculture, v. 20, p. 633–640.